UNIVERSITY OF GHANA
COLLEGE OF BASIC AND APPLIED SCIENCES

SINGLE H/H_2 ADSORPTION ON TRANSITION METAL DISULPHIDES (TMS_2)

MICHAEL ANAKWAH

DEPARTMENT OF PHYSICS

August, 2022

UNIVERSITY OF GHANA
COLLEGE OF BASIC AND APPLIED SCIENCES

SINGLE H/H_2 ADSORPTION ON TRANSITION METAL DISULPHIDES (TMS_2)

BY
MICHAEL ANAKWAH

(ID. NO. 10415460)

This thesis is submitted to the University of Ghana, Legon in partial fulfilment of the requirement for the award of **MPHIL in PHYSICS Degree.**

August, 2022

Declaration

I hereby declare that, this thesis is my work which contains no material previously published or written by another person nor any material which has been accepted for the award of any other degree or diploma of the university or any other institute of higher learning, except where due acknowledgment has been made in the text.

Student

Anakwah Michael

Signature: .....

Date: 23-10-2023

Supervisors

Dr. Gebremedhin H. Gebreyesus

Signature: .....

Date: 23-10-2023

Dr. Kingsley Obodo

Signature: .....

Date: 24-10-2023

Acknowledgements

My heartfelt gratitude goes to my two supervisors, Dr Gebremedhin H. Gebreyesus and Dr Kingsley Obodo, who guided and motivated me from the beginning to the end of this project. I would also like to thank the graduate committee members for making my defense a success, as well as for your insightful critiques and suggestions.

Finally, I would like to thank my family for their unwavering support and encouragement.

Abstract

2D transition metal disulphides have gained a lot of research interest due to their fantastic electrical, optical, magnetic, and mechanical properties which makes them recommended for electrical and optical applications. More interestingly, they have been proposed as suitable alternatives to Pt hydrogen evolution reaction catalysts as they also exhibit layered structures in which the layers interact through Van der Waals forces. Semiconducting transition metal disulphides in bulk are indirect band gap materials whereas their monolayers exhibit direct band gap. Metallic (1T) phase of transition metal disulphides has been widely studied due to their higher hydrogen evolution reaction activity and the tremendous optical and electrical applications it offers. The successful fabrication of bilayer heterostructures of 1T transition metal disulphides will open opportunities for industry scale HER catalysts and electrical devices applications. In this work, we have analyzed structural, electronic, and energetic properties of monolayer 1T-Mo S_2, 1T-Re S_2, 1T-W S_2 and 1T-Pd S_2 using density functional theory calculations. Bilayer heterostructures including 1T-MoS_2-PdS_2, 1T-WS_2-PdS_2, 1T-PdS_2-ReS_2, 1T-MoS_2-WS_2 and 1T-WS_2-Re S_2 have been formed and again density functional calculations have been performed on these heterostructures. It was found that 1T-MoS_2-PdS_2, 1T-WS_2-PdS_2 and 1T-PdS_2-ReS_2 can be formed spontaneously and also the bilayer heterostructures composed of two metallic monolayers predict a novel metallic van der Waal solids that might be used in future 2D nanomaterials. Finally, 1T-MoS_2-PdS_2, 1T WS_2-PdS_2 were found to be the most stable with adsorption free energy close to zero and can serve as suitable catalysts for hydrogen evolution reaction.

List of Abbreviations

DFT Density Functional Theory

DOS Density of State

GGA Generalized Gradient Approximation

LDA Local Density Approximation

PBE-sol Perdew-Burke-Ernzerhof-solution

PWPP Plane Wave pseudopotentials

Quantum ESPRESSO opEn-Source Package for Research in Electronic Structure, Simulation and Optimization

SCF Self Consistent Field

MoS2 Molybdenum disulphide

ReS2 Rhenium disulphide

PdS2 Palladium disulphide

WS2 Tungsten disulphide

List of Figures

List of Tables

Table of Contents

Chapter 1

Introduction

1.1 Overview

The estimated increase in global energy demand from 17TW in 2010 to 27TW by 2040 (US EIA, 2013) shows an exponential growth. Utilizing renewable and clean energy sources is crucial given the depletion of fossil fuels and rising environmental pollution, which has long-lasting repercussions on climate change. Since hydrogen has the highest combustion energy of all chemical fuels and only produces water as a byproduct of combustion, clean hydrogen energy is currently experiencing unheard-of political and commercial momentum. Since the current method of producing hydrogen emits carbon dioxide, we must look for workable substitutes that wouldn't result in the release of greenhouse gases.

These solutions can be achieved by finding the best catalysts to help speed up the hydrogen evolution reaction. As different reactions may require different energies to occur, catalysts play an important role by lowering this energy. The production of hydrogen through water-splitting can be achieved using either photo-catalysis or electro-catalysis.

Due to its high exchange current and relatively modest Tafel slope, platinum (Pt) and its alloys are now regarded the most active and stable catalysts for hydrogen evolution reactions (Seh et al (2017)). Aside from the fact that Pt is scarce, it is also exceedingly costly, making it inefficient to create realistic and scalable hydrogen amounts. As a result, there has been a large research effort directed at using low-cost earth abundant catalysts to replace the precious metal (Pt) (Westholm et al., 2018). According to recent research, MoS2 exists in two phases: the 2H phase and the IT phase. The 2H phase is metallic, while the

1T phase is semiconductor (Xu et al., 2018). The metallic 1T phase has outstanding HER catalytic activity, although the 2H semi-conducting phase is likewise catalytically inert, and the catalytic activity correlates to the unsaturated edges of S and Mo atoms and may be likened to a perfect Pt catalyst (Cai et al., 2017). This great understanding has encouraged some research strategies that focuses on maximized exposing of edge sites into nano-sheets MoS2 through synthesizing nanoparticles, defective nano-sheets and its corresponding experimental results also verify that the exposed edges play an important role in HER. Another strategy also seeks to enhance intrinsic catalytic activity of the edge sites by chemical doping. The 1T polytypes of transition metal disulphides are known to have large surface area, good conductors and enhanced photo and electro-catalytic capabilities (Cai et al., 2017). Due to the enormous, interesting properties exhibited by 1T polymorphs of transition metal disulphides, this work focuses on studying the intrinsic structural, electronic and mechanical properties of Transition metals (Re, Mo, Pd, W) disulphides as well their hetero structures through computational methods.

1.2 Hydrogen Evolution Reaction

Two mechanisms namely the Volmer-Tafel and the Volmer-Heyrovsky are needed to achieve hydrogen evolution reaction in below reactions:

$$\text{Volmer Step: } H^+ + e^- \rightarrow H_{ads} \quad (1)$$

This step involves the adsorption of a hydrogen ion (H^+) and an electron (e^-), forming an adsorbed hydrogen atom (H_{ads})

$$\text{Heyrovsky Step: } H^+ + H_{ads} \rightarrow H_2 \quad (2)$$

This step involves the combination of a hydrogen ion (H^+) with an adsorbed hydrogen atom (H_{ads}), leading to the formation of molecular hydrogen (H_2).

$$\text{Tafel Step: } 2H_{ads} \rightarrow H_2 \quad (3)$$

This step involves the recombination of two adsorbed hydrogen atoms ($2H_{ads}$), resulting in the production of molecular hydrogen (H_2).

The volmer step is the first reaction to happen proceeded by either the Tafel or Heyrovsky. Clearly, regardless of the pathway taken by Hydrogen evolution reaction, both mechanisms Volmer-Tafel and the Volmer-Heyrovsky show that there is surface adsorbed hydrogen at electrode. This implies that the *adsorption free energy* of hydrogen plays a decisive role in the determination of the catalytic activity of the catalysts(Cai et al., 2017).

H_{ads} is related the adsorption free energy of H

$$\Delta G_H = \Delta E_{ads} + \Delta E_{ZPE} + T\Delta S_H \quad (4)$$

where ΔE_{ads} is the adsorption energy of hydrogen, ΔE_{ZPE} is the difference in zero-point energy between hydrogen in the adsorbed and gas phase state, T is the temperature in Kelvin and ΔS_H is the change in entropy between hydrogen in the adsorbed and gas phase.

According to the Sabatier principle, an ideal catalyst must bind to the reactant at an intermediate strength, i.e., neither too weak nor too strong (Cai et al., 2017). If the hydrogen to surface bond is too weak, the adsorption step (Volmer-step) will limit the overall reaction rate. Also, if the hydrogen surface bond is too strong, the reaction-desorption (Tafel/Heyrovsky) step will limit the reaction rate. Optimal HER catalysts have hydrogen adsorption energies close to $\Delta G_H = 0$; i.e., binding neither too strongly nor weakly(Cai et al., 2017).

In order to maximize the rate of Hydrogen Evolution reaction, a catalyst with appropriate surface properties must be used. Previous studies have reviewed several materials as active Hydrogen evolution reaction (HER) catalysts including Platinum, metal oxides, metal phosphides and metal Sulphides as shown in Figure 1.1

Figure 1.1 Exchange current density as a function of hydrogen adsorption free energy for various HER catalyst materials.

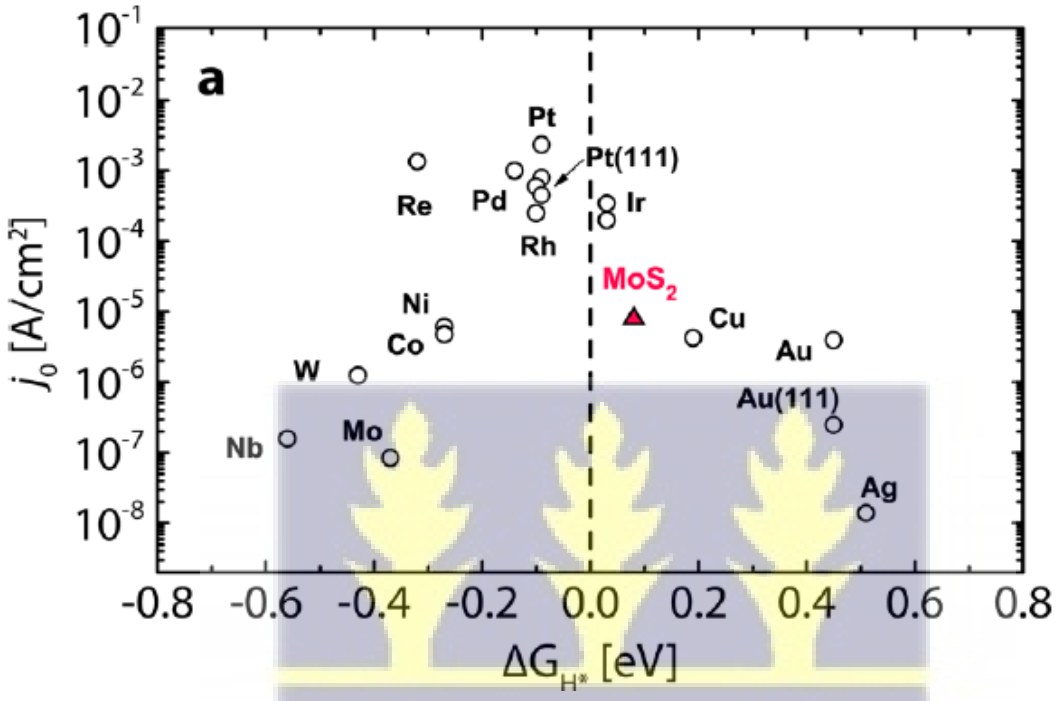

(a) The experimental" volcano *plot*" for the HER is shown and Pt, with slightly negative hydrogen absorption energy has the highest HER activity(Cai et al., 2017)

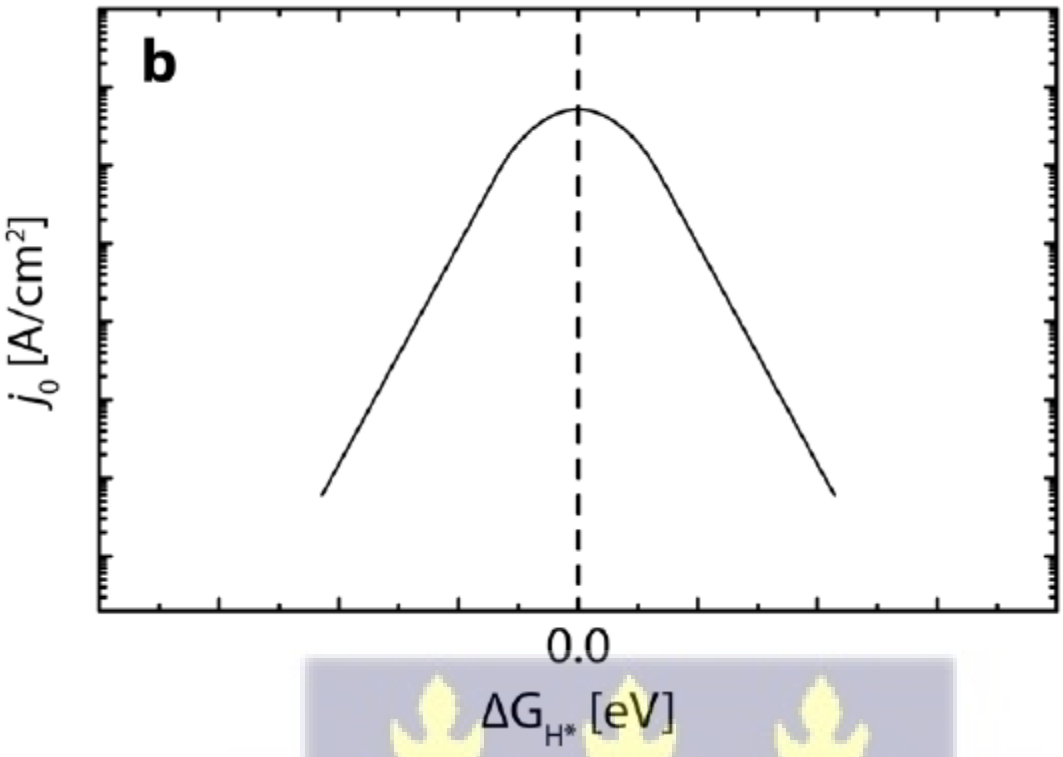

(b) The theoretical HER volcano, adapted from Parsons, predicts catalysts with hydrogen binding energy equal to zero will have the highest activity (Jaramillo et al 2007)

Even though Platinum remains the gold standard for highly efficient catalyst for hydrogen evolution reaction, cost is a major barrier towards their commercial viability. It has therefore become prudent to find more abundant and relatively cheaper materials that exhibit high photocatalytic activity towards hydrogen evolution reaction.

Ever since Titanium dioxide was used as the first semiconductor for photocatalytic water splitting there has been several attempts to develop efficient photo catalysts including metal carbides, metal alloys, carbon nanotubes and others. However, there remains a primary challenge of ridding photo catalyst of poor efficiency due to the recombination possibilities of electrons and holes.

Recent advancement of graphene technology and the exfoliation of ultrathin materials have directed tremendous interest towards the exploration of 2D materials and the fabrication of fewer layer or monolayer sheets to control the charge carrier recombination process(Cai et al., 2017). Thin materials at the atomic scale, like transition metal dichalcogenides (TMDCs), have been extensively studied for their intriguing electron and optical properties, as well as their ability to be synthesized across large areas. TMDCs have the structural formula X-M-X where (M is the transition metal and X is S, Se, Te) due to the distinctive crystal structure and rich chemistry. In addition, 2D materials can also manifest distinct properties through the formation of heterostructures, surface formation and others (Tan et al., 2017).

This work focuses on monolayers, bilayers and heterostructures of transition metal disulphides (TMS2), (a category of the TMDCSs) as photo-catalysts for hydrogen evolution reaction. A variety of reasons for the choice of these materials are stated below.

First, numerous earlier investigations have demonstrated that the indirect to direct band gap transition occurs during the material transitions from bulk to many layers in semiconductor transition metal disulphides such as MoS2 and WS2 as well as other TMDCs like MoSe2 and WSe2. Additionally, different transition metals have different populations of the d-orbitals, which results in a range of electron properties from semi-conductors, insulators, and superconductors. This makes them appealing for technological research in a variety of fields, including photocells, photo detectors, and various electronic devices.

Technology applications have taken a strong interest in TMDCs due to their effectively high mobility of charge carriers. Finally, the photocatalytic TMS_2 is crucial for splitting water after receiving solar radiation due to its superior band gap. It has been observed in recent experiments that MoS_2 is cost effective and has a better HER catalytic efficiency compared to most non-precious metals. Other studies have also shown that the H_2 phase of MoS_2 is responsible for its catalytic activity and requires a carefully

good design of material to expose an increased number of its edge sites. Improved catalytic activity has also been reported for Pd doped monolayer of WS_2 and metal edge doping in MoS_2. (Xu et al., 2018)

These various findings prepare the background for the motivation of Single H/H2 Adsorption on transition metal disulphides focusing on the hydrogen evolution reaction activity on monolayers and bilayers of MoS_2, WS_2, PdS_2, ReS_2 as well heterostructures of these TMS_2 such as MoS_2-WS_2, MoS_2-PdS_2 and MoS_2-ReS_2, WS_2-PdS_2, WS_2-ReS_2 and PdS_2-ReS_2 using density functional theory based electronic structure calculations. We have determined electronic, magnetic, structural, and optical properties and performed HER on these surfaces.

1.3 Specific Objectives

The aim of this research work is to study structural, energetic and electronic properties of specific monolayer 1T-transitional metal disulphides including MoS_2, WS_2, PdS_2, ReS_2. Secondly, to form bilayers of heterostructures of the transition metal disulphides including MoS_2-WS_2, MoS_2-PdS_2 and MoS_2- ReS_2, WoS_2-PdS_2, WS_2-ReS_2 and PdS_2-ReS_2 and study their properties to be able to determine which of these heterostructures can be formed spontaneously. The electronic and structural properties are analyzed to determine whether these materials can be used as good catalysts.

1.4 Outline of this work

The structure of the thesis is organized as follows:

• Chapter 1 presents the overview of the transition metal disulphides and hydrogen evolution reaction

• Chapter 2 presents an in-depth theoretical framework of an understanding of Concepts of solids and density functional theory.

• Chapter 3 the discussion of theoretical methods employed in this study is presented.

• Chapter 4 The detail analysis of results are discussed in this chapter

• Chapter 5 Presents conclusion and future perspectives

Chapter 2

Theoretical Framework

2.1 Crystal Lattices

A crystal lattice is a repeating three-dimensional arrangement of atoms, ions, or molecules in a solid substance. In crystallography, crystal structure is a description of the ordered arrangement of atoms, ions, or materials in a crystalline material. Ordered structures naturally form repeated symmetric patterns along the principal directions of three-dimensional space in matter. The unit cell of the structure is the smallest group of materials that constitute the repeating pattern. The unit cell completely reflects the symmetry and structure of the entire crystal, and it is built up by repetitive translation of the unit cell along its principal axes. The translation vectors define the nodes of a Bravais lattice.

The Bravais lattice is a collection of discrete points with just an arrangement and orientation that seem same from every viewpoint. Bravais lattice may be defined as any array of three-dimensional discrete points that is arranged in such a way that when seen from any point, it appears precisely the same regardless of whatever point it is viewed from. Mathematically, a set of points that the position vector $\hat{R}$ consists of is the Bravais vector as represented below.

$$\hat{R} = \sum_i n_i a_i \tag{4}$$

where a_i consists of all vectors in the same plane and n_i are range through all integer values. The vectors $a_i$that appears in equation (4) are the primitive vectors which are known to span the entire lattice.

The unit cell is also an important concept in crystal lattices. It is the simplest repeating unit in a crystal. Each unit cell is defined in terms of lattice points – the points in space about which the particles are free to vibrate in the crystal. Unit cells can be classified into primitive and conventional unit cell. The difference between the primitive and the conventional unit cell is that, in the case of primitive, it is a

space cell centered on a lattice point that, when moved using the Bravais lattice vectors, fills the whole space of the crystal without overlapping. There is another kind of primitive cell known as the Wigner-Seitz cell for every Bravais lattice. The lattice point in the Wigner- Seitz cell lies at the center of the cell, and the form of most Bravais lattices is a parallelogram or parallelepiped. The Wigner- Seitz cell of a reciprocal lattice in momentum space is known as the Brillouin zone.

2.1.1 Reciprocal Lattices

Because crystal structures are periodic, they can be handled in the reciprocal lattice space. The reciprocal lattice is a representation of another lattice, typically the Bravais lattice, using its Fourier transform. It is natural to compare Bravais lattice in the reciprocal space with periodic plane waves. Reciprocal lattice points are represented below

$$K = k_1\hat{b}_1 + k_2\hat{b}_2 + k_3\hat{b}_3 \qquad \forall\, k_1, k_2, k_3 \in \mathbb{Z} \tag{5}$$

Where K *denotes the reciprocal lattice points and* b_1, b_2 *and* b_3 are the reciprocal primitive vectors given by below

$$\hat{b}_1 = 2\pi \frac{a_2 \times a_3}{a_1 \cdot (a_2 \times a_3)} \tag{6}$$

$$\hat{b}_2 = 2\pi \frac{a_3 \times a_1}{a_1 \cdot (a_2 \times a_3)} \tag{7}$$

$$\hat{b}_3 = 2\pi \frac{a_1 \times a_2}{a_1 \cdot (a_2 \times a_3)} \tag{8}$$

These equations must satisfy the condition that

$$e^{iK.R} = 1 \tag{9}$$

It can be said that the first Brillouin zone is the Wigner-Seitz cell of the reciprocal zone.

2.1.2 The Bloch's Theorem

Bloch formulates a crystal system consisting of electrons that lack interaction within a periodic potential, as illustrated below.

The Hamiltonian of single electron state Ψ is given by

$$-\frac{\hbar^2}{2m}\nabla^2 + U(\hat{r}) \tag{10}$$

Where $U(\hat{r} + \boldsymbol{R}) = U(\hat{r})$ for all **R** in that exists in a Bravais lattice,

$$\Psi_{nk}(\hat{r}) = e^{ik.\hat{r}} u_{nk}(\hat{r}) \tag{11}$$

where

$$u_{nk}(\hat{r} + \hat{R}) = u_{nk}(\hat{r}) \tag{12}$$

For all $\hat{R}$ in the Bravais lattice. Alternatively, one can choose the eigenstates of the Hamiltonian so that each Ψ is associated with a wave vector k:

$$\Psi(\hat{r} + \hat{R}) = e^{ik.R}\Psi(\hat{r}) \tag{13}$$

The equation expresses the relationship between the wave function at a position $\hat{r} + \hat{R}$ and the wave function at the original position $\hat{r}$ in terms of a phase factor $e^{ik.R}$

Even though the proof Bloch's theorem is reliant on periodicity oh Hamiltonian, it is silent about the wave vectors allowed values. When the Born-Karman boundary condition is imposed, it can be shown clearly that the each allowed k-vector space is given by

$$V_k = \frac{(2\pi)^3}{N} \tag{14}$$

Where V_k is the volume /k point, N being the total number of primitive cells. The allowed wave vectors behave as a continuum since the primitive cells in a crystal is very large. Despite that the allowed values of k vector span over the entire crystal, the key interest can be restricted to the first Brillouin zone k and can be written as

$\hat{k} = k' + \hat{K}$ where K is the reciprocal lattice vector and k' is inside the Brillouin zone.

2.1.3 Band Structure

As the wave function is determined by the wave vector, electronic energies are likewise affected by the wave vector. Consequently, the energy relationship can be expressed as follows: the band structure is defined by energies that depend on the wave vectors (k-vector). Within the first Brillouin zone, the wave vector is plotted across high symmetry points.

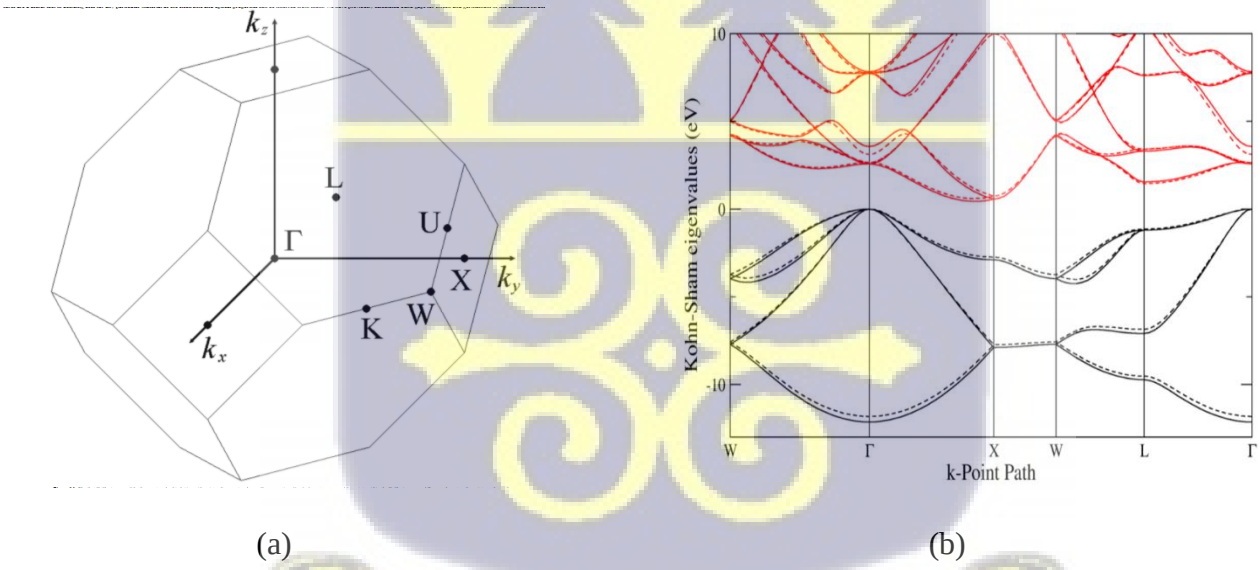

(a) (b)

Figure 2.1 (a) The first Brillouin zone of the face centered cubic lattice. (b) the band structure of silicon using Local Density Approximation (dashed lines) and Weighted Density Approximation (thick lines) plotted along high symmetry lines.

2.1.4 The Fermi Energy

Assuming we have an N-electronic system, the electrons can only occupy a portion of the band structure. Electrons are known to follow the Pauli's exclusion principle, which states that no two electrons may occupy the same state, suggesting that electrons will fill the energy bands from lowest to greatest energy. The Fermi energy is the energy that exists between the greatest occupied energy level and the lowest vacant energy level.

There are two primary methods for filling the bands:

1. There may be partly filled bands in which the Fermi energy will interpenetrate one or more bands.
2. All the occupied bands may be filled with energy that falls between the most and least occupied bands.

The electronic properties of materials depend on how the bands are filled. In the case where the conduction band overlaps with the valence bands causing an intersection with the fermi energy, the material is metallic. In case 2 above, the material behaves as a semiconductor or an insulator depending on the energy gap (Martin et al. 2008)

Materials' electronic characteristics are determined by how the bands are filled. The material is metallic when the conduction band overlaps with the valence bands, resulting in an intersection with the fermi energy. Depending on the energy gap, the material in Case 2 above acts as a semiconductor or an insulator.

2.2 Density Functional Theory (DFT)

DFT is a successful theory to calculate the electronic structure of atoms, molecules, and solids. Its focuses on a quantitative understanding of the material from the fundamental laws of quantum mechanics. In order to solve the Schrodinger equation for a system of N electrons moving in an external potential (typically generated by the nuclei), the traditional electronic structure methods seeks to find approximate

solutions to the Schrodinger equations. This approach becomes less effective for large numbers N due to the fact that the resulting wave becomes more complicated as N increases. Also the computational effort grows very rapidly for increasing values of N and becomes prohibitive to make calculations for larger systems. Density functional theory (DFT) employs a very different approach, instead of the many-body wave function, the one-body density is used as the fundamental variable. Since the density n(r) is a function of only three spatial coordinates (rather than the 3N coordinates of the wave function), density-functional theory is computationally feasible even for large systems.

2.3 The Many Body Problem

Fundamentally the challenge in solving the many body problem is in dealing with the various interactions between the electrons and neutrons (i.e. electron-electron, electron-nuclei, and nuclei-nuclei, interactions of all known and unknown potentials). The electronic properties of such a system that is made up of N electrons can be obtained when the many-body Schrodinger equation is solved

$$\hat{H}\Psi(\hat{r}_1, \hat{r}_2, \dots, \hat{r}_n, \hat{R}_1\hat{R}_2 \dots) = E\Psi(\hat{r}_1, \hat{r}_2, \dots, \hat{r}_n, \hat{R}_1\hat{R}_2 \dots) \quad (15)$$

Where r_i and R_i is the position vectors of electrons and nuclei respectively. $\hat{H}$ is the Hamiltonian of the system which is given by

$$\hat{H} = -\frac{\hbar^2}{2m}\sum_i {\nabla_i}^2 - \sum_{i,I}\frac{e^2 Z_I}{|r_i - R_I|} + \frac{1}{2}\sum_{i\neq j}\frac{e^2}{|r_i - r_j|}$$

$$-\frac{\hbar^2}{2M_I}\sum_I {\nabla_I}^2 + \frac{1}{2}\sum_{I\neq J}\frac{e^2 Z_I Z_J}{|R_i - R_j|} \quad (16)$$

Where $m_e$the electron is mass, M_I is the mass of the Ith ion, ħ is the Planck's constant/2π , Z_I is the atomic number of the Ith ion and e is the electronic charge.

The terms in the Hamiltonian are described below

The electronic and ionic kinetic energies are respectively given as

$$\hat{T} = \frac{\hbar^2}{2m_e}\sum_i \nabla_i{}^2 \tag{17}$$

$$\hat{T}_I = \frac{\hbar^2}{2M_I}\sum_I \nabla_I{}^2 \tag{18}$$

The potential energy resulting from the electron –electron interactions is

$$\hat{V}_{e-e} = \frac{1}{2}\sum_{i\neq j}\frac{e^2}{|r_i - r_j|} \tag{19}$$

The potential energy resulting from electron- ion interaction is given by

$$\hat{V}_{e-I} = \sum_{i,I}\frac{e^2 Z_I}{|r_i - R_I|} \tag{20}$$

The potential energy resulting from the ion –ion interaction is given by

$$\hat{V}_{I-I} = \frac{1}{2}\sum_{I\neq J}\frac{e^2 Z_I Z_J}{|R_i - R_j|} \tag{21}$$

Utilizing many-body approximations is crucial to restrict the system to a small number of particles , enabling an accurate computation of the Hamiltonian. Modeling, this system with high precision would result in an impractical and excessively high computational cost. One of the initial approximations employed for this purpose is the Born-Oppenheimer approximation (Kohn, 1999).

2.3.1 Born-Oppenheimer Approximation

The Born-Oppenheimer Approximation realizes that the electrons are much lighter and moves faster than the nuclei (ions) so that one motion of the two degrees of freedom, and hence the kinetic energy term of the nuclei can be ignored. This approximation will reduce the problem to

$$\hat{H} = -\frac{\hbar^2}{2m}\sum_i \nabla_i{}^2 - \sum_{i,I}\frac{e^2 Z_I}{|r_i - R_I|} + \frac{1}{2}\sum_{i\neq j}\frac{e^2}{|r_i - r_j|} + \frac{1}{2}\sum_{I\neq J}\frac{e^2 Z_I Z_J}{|R_i - R_j|} \quad (22)$$

Or simply written as

$$\hat{H} = \hat{T} + \hat{V}_{e-e} + \hat{V}_{e-I} + \hat{V}_{I-I} \quad (23)$$

Even though some simplification is achieved by the Born-Oppenheimer approximation it is still not possible to solve the many body problem exactly for more than a complicated single atom. In principle, it is very difficult to solve the electron- electron interactions in the sense every electron at every point in time feels or is affected by a slight motion of any of the electrons and this what gives rise to the collective and correlated complexity of the many body problem. More so, the wave function Ψ has a 3N degree of freedom for N electrons. The complexity of solving the wave function is addressed by density functional theory. The quest to calculate accurately the electronic structure of real materials birthed the Density Functional Theory (DFT). Early works of P. Hohenberg and W. Kohn in 1964 demonstrated profoundly that one can express the total energy of a system as a functional of the electron density n(r), $E = E[n(\vec{r})]$ where the exact form of $E[n(\vec{r})]$ is unknown (Hohenberg & Kohn, 1964). Kohn and Sham later constructed a Schrodinger like equation that could solve a single electron problem in a mean field manner (Kohn & Sham, 1999). DFT employs several approximations to calculate the electronic structure and by extension the ground state properties of materials can be calculated such as structural, magnetic, optical, and mechanical.

2.3.2 The Hohenberg-Kohn Theorems

Density Functional Theory is based on the Hohenberg and Kohn theorems, which indicate that the ground state electron density $\left(n_o((\vec{r}))\right)$.may completely predict the many-body electron problem. In theory, this theorem permits the substitution of the number of vectors of the number of electron wave functions with a problem that relies on a scalar function $n((\vec{r}))$. This crucial substitution becomes more significant as the number of atoms in a system grows, and it is the primary reason DFT was successful.

The following theorems apply to a system that is non-degenerate.

Theorem I- Any system of particles that exist in an external potential $V_{ext}(\vec{r})$, the potential $V_{ext}(\vec{r}\,)$ i uniquely determined, except for a constant, by the ground state of particle density $n_o(\vec{r})$.

Theorem II- A universal functional for the energy $E = [n]$ in terms of the density $n(\vec{r}\,)$ can be defined valid for any external potential $V_{ext}(\vec{r}\,)$ for any particular $V_{ext}(\vec{r})$, the exact ground state energy is the global minimum value of this functional, and the density $n(\vec{r}\,)$ that minimizes the functional is the exact ground state density $n_o(\vec{r})$.

The theorems mean the external potential $V_{ext}(\vec{r})$ completely define the quantum problem. Also the wavefunctions are in principles uniquely determined via the Schrodinger equation. The energy and everything else is thus a functional of the external potential $V_{ext}(\vec{r})$. The external potential determines uniquely the charge density and the charge density determines uniquely the external potential.

The functional described in Theorem II is the total energy functional defined as

$$E[n] = F_{HK}[n] + \int d^3r\ V_{ext}(\vec{r})\, n(\vec{r}) + E_{I-I} \tag{24}$$

Where $F_{HK}[n]$ is defined from the many body problem as

$$F_{HK}[n] = \langle \hat{T} \rangle + \langle \hat{V}_{e-e} \rangle \tag{25}$$

With $\hat{T}$ and $\hat{V}_{e-e}$ given by equations which is a **universal functional**. E_{I-I} describes the ion-ion interactions.

2.3.3 Kohn-Sham Equations

The challenge of the Hohenberg-Kohn theorems is that, even though the theorems define a functional of total energy that is only dependent on the electron density in principle, the universal functional $F_{HK}[n]$ is not known in any method that does not include the electron many-body wave function explicitly. Instead of using the total energy functional directly, Kohn and Sham proposed a non-interacting unique mapping reference approach. In this reference system, electrons do not interact and dwell in an external potential so that their ground state charge density is like the interacting system's ground state charge density. Based on the assumptions stated above, the energy functional developed for the non-interacting system, which for doubly occupied electronic wave functions I is represented as follows:

$$E[\{\Psi_i\}] = -\sum_i \int \Psi_i \nabla^2 \Psi_i \, d^3\vec{r} + \int V_{ext}(\mathrm{r})\mathrm{n}(\mathrm{r})\mathrm{d}^3\vec{r} + \frac{1}{2}\int \frac{n(r)n(r')}{|\vec{r}-\vec{r}'|} d^3\vec{r} d^3\vec{r}'$$

$$+E_{xc}[n(\vec{r})] + E_{I-I}(\{\vec{R}_I\}) \qquad (26)$$

Ψ_i are the non-interacting systems wavefunction, r is the position vector of the electron, E_{I-I} is the already defined ion-ion energy functional in (26) and E_{xc} is the new term called the exchange correlation functional. R_I is the position vectors of the ions and $n(\vec{r})$ is the electron density.

The electron density $n(\vec{r})$ for the non-interacting may be written as:

$$n(\vec{r}) = 2\sum_i |\Psi_i|^2 \qquad (27)$$

Putting together the terms in equation, we obtain

$$E = T_s[n] + \int V_{ext}(\vec{r})\mathrm{n}(\vec{r})\mathrm{d}^3\vec{r} + E_{Hatree}[n] + E_{xc}[n] + E_{I-I}$$

Where $T_s[n]$ is the kinetic energy of the non-interacting system and E_{Hatree} is the electron-electron interaction term without the exchange and correlation effects. These are defined by

$$T_s[n] = -\sum_i \int \Psi_i \nabla^2 \Psi_i \, d^3\vec{r} \tag{28}$$

$$E_{Hatree}[n] = \frac{1}{2}\int \frac{n(\vec{r})n(\vec{r}')}{|\vec{r}-\vec{r}'|} d^3\vec{r} d^3\vec{r}' \tag{29}$$

The effects of exchange and correlation of the many original many body wave function have been put in the exchange-correlation functional in the Kohn-Sham equations. If the exchange– correlation functional were known, the ground state energy would have been obtained by minimizing equation (29) leading to yielding of the density of the many-body problem when the Kohn-Sham equation is solved.

The minimization of the Kohn-Sham energy with respect to the electron density n(r) and applying the chain rule, below is obtained

$$\frac{\delta E[\{\Psi_i\}]}{\delta \Psi_i^*} = \frac{\delta T_s[n]}{\delta \Psi_i^*} + \left[\frac{\delta E_{ext}}{\delta n(\vec{r})} + \frac{\delta E_{Hatree}}{\delta n(\vec{r})} + \frac{\delta E_{xc}}{\delta n(\vec{r})}\right]\frac{\delta n(\vec{r})}{\delta \Psi_i^*} = 0 \tag{30}$$

Which is subject to the normalization

$$\langle \Psi_i^* | \Psi_k \rangle = \delta ik \tag{31}$$

This yields the Kohn Sham equation

$$\left[-\frac{1}{2}\nabla^2 + V_{ext}(r\vec{r}) + V_{Hatree} + V_{xc}\right]\Psi_i = \varepsilon_i \Psi_i(\vec{r}) \tag{32}$$

Where V_{Hatree} and V_{xc} can be seen clearly from equation as

$$V_{Hatree} = \frac{\delta E_{Hatree}}{\delta n(\vec{r})} \tag{33}$$

$$V_{xc} = \frac{\delta E_{xc}}{\delta n(\vec{r})}$$

Equations (32) and (33) helps us formulate and implement self-consistent field (SCF) methods using approximate exchange correlation functionals. The SCF method is represented in the flow scheme below

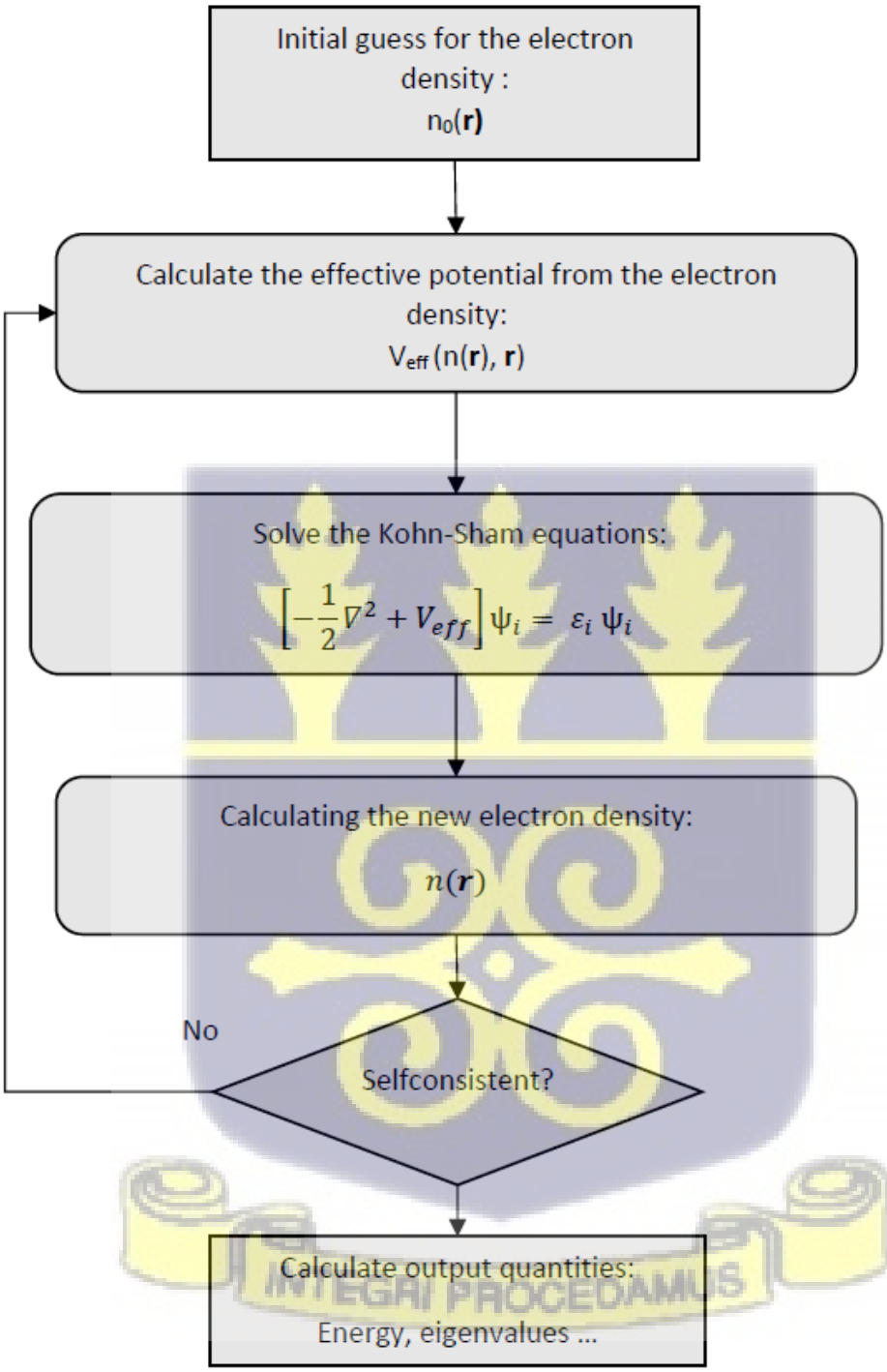

Figure 2.2 A flow chart that describes the implementation of SCF

2.3.4 The Exchange Correlation Functional

The exchange correlation functional in density functional theory substitutes the effects of correction and exchange in the original many-body problem. There are no analytic forms for the exchange correlation yet, therefore feasible approximations (i.e., the construction of exchange correlation functionals) are required to make DFT an usable tool.

The first approximation developed was the Local Density Approximation (LDA). An approximation of the exchange correlation of a "homogeneous" electron gas in the LDA, where the density of the electron gas is assumed to be the same as the local electron density:

$$E_{xc}^{LDA} = \int d^3r n(r) \varepsilon_{xc}(n(r)) \tag{34}$$

ε_{xc} is the exchange-correlation energy density of a homogenous electron gas with a uniform positive background charge so that the system is electrically neutral. The exchange correlation energy can be splitted into the exchange term and the correlation term

$$\varepsilon_{xc}(n(r)) = \varepsilon_c(n(r)) + \varepsilon_x(n(r)) \tag{35}$$

The exchange term of the exchange correlation energy can be expressed in an analytic form. However, there exist no analytic formula for the correlation term, rather, the value of the correlation energies have been computed numerically by employing quantum Monte Carlo methods making it possible to obtain accurate, exchange correlation energies.

There have been so many attempts to improve upon the Local Density Approximation. Among these are a class of functionals depending on the local density and local gradient $\nabla n(\mathrm{r}^{\rightarrow})$ of the electron density called the generalized gradients approximation (GGA):

$$E_{xc}^{LDA} = \int d^3 r n(r) \varepsilon_{xc}\left(n(r), \nabla n(\mathrm{r}^{\rightarrow})\right) \quad (36)$$

Where ε_{xc} is the exchange correlation energy and the form it takes depends on which GGA method that is selected. There are many flavors of GGA including BP88, PW91, PBE etc. which yields similar but slightly different. These are the most currently used functionals in calculations with excellent price-performance ratio but with some shortcomings.

2.4 Pseudopotentials and Plane waves

2.4.1 Pseudopotentials

Because valence electrons operate as free particles (non-interacting) distant from the core, it is logical to represent the valence wave functions using plane waves. However, owing to the densely coupled core electrons, the wave functions fluctuate quickly around the core. This indicates that a large number of plane waves are needed to accurately depict the valence electrons wave functions. Using so many plane waves to solve the Kohn-Sham equation leads in an extremely computationally costly technique that is not practical until additional acceptable approximations are used. The primary goal of using pseudopotentials is to substitute the high coulomb potential caused by densely coupled core electrons with a lesser effective potential.

Excluding core electrons from computations indicates that we lose most of the knowledge about what happens at the inner core; yet, most physical properties rely mostly on valence electrons and maintain a high accuracy in physical property prediction even when core electrons are excluded.

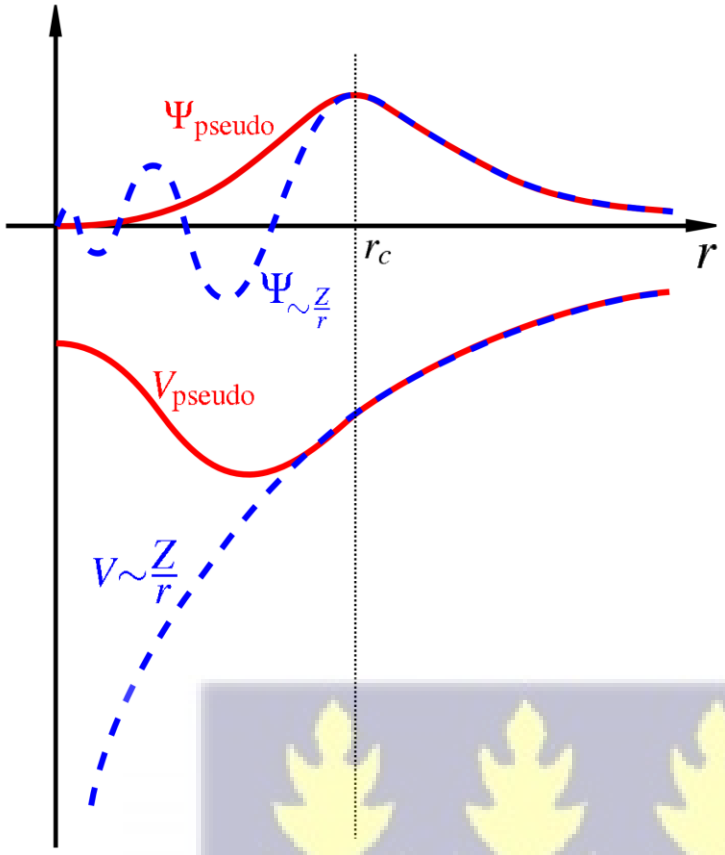

Figure 2.3 A depiction of the pseudopotential and its associated pseudo wavefunction (solid red line), as well as the theoretical Coulomb potential and valence electron waveform (dotted blue line). The image was obtained from (Quester., 2018)

2.4.2 Ultrasoft pseudopotentials and Projector augmented-wave functions

The orthogonal plane waves (OPW) approach is used in the Projector augmented-wavefunction (PAW), but it is better suited to total energy estimates. The PAW's main concept is to describe the valence electron wavefunction using pseudo wavefunctions and a linear transformation utilizing projector functions.

$$|\Psi\rangle = T|\varphi\rangle \tag{38}$$

Where Ψ is the valence electron wave function, T is the linear transformation operator and φ is the pseudo valence electron wave function.

We may expand the pseudo and valence electron wave function using partial wave functions

$$|\Psi\rangle = C_n|\Psi_n\rangle \tag{39}$$

$$|\varphi\rangle = C_n|\varphi_n\rangle \tag{40}$$

Equations (38), (39) and (40) imply the existence of projector functions (P_n) around each core full filling:

$$\langle P_a|\varphi_n\rangle = \delta_{a,n} \tag{41}$$

Where P_a is the projector is function and $\delta_{a,n}$ is the kronecker delta function. This results in below form for the linear transformation:

$$T = 1 + \sum_n (|\Psi\rangle - |\varphi\rangle)\langle P_n| \tag{42}$$

Chapter 3

Methodology

First principle calculations used in this work were performed in Quantum Espresso. Generalized global approximation with Perdew-Burke Ernzerhof modified for solids (PBE-Sol) functional describing the exchange and correlation energy was applied. First, the convergence of structural optimization and calculation of the physical properties of the materials were tested with respect to the plane wave cut-off energy and k-points. The Monkhorst-Pack grid of 8x8x1 (Monkhorst & Pack, 1976) was applied to sample the Brillouin zone, also optimized vacuum distance of approximately 25Å to prevent any interaction between periodic images in the z-plane. For the electronic band structure and density of states calculation, a more refined Monkhorst -Pack states were used. In this work, we have studied structural, energetic and electronic properties of monolayers and heterostructures of transition metal disulphides. Quantum espresso implementation of Density functional theory (DFT) was used for the computation of structural and electronic properties of monolayer and hetero-structures of 1T prototypes of transition metal disulphides namely PdS_2, WS_2, ReS_2, ReS_2-WS_2, MoS_2-WS_2, PdS_2-WS_2, ReS_2-PdS_2. The Generalized Gradient Approximation (GGA) of the exchange correlation energy and pseudopotentials were applied to these calculations. Brillouin zone sampling was also done using the Monkhorst-Pack approach where 14x14x2 and 16x16x2 were used for the monolayer and hetero-structures respectively. We first performed variable-cell relaxation computation for all the materials to obtain the optimized lattice parameters of these materials where the results are discussed in section 4.1 below. Self-consistency field (scf) calculations were performed for all the materials to obtain their total energies.

3.1 Structural Optimization Computation

Structural optimization for all the materials used in this project is performed to determine the lattice constants, atomic distance and angles and bond lengths. Variable cell relaxations was carried out until forces acting on each atom are less than 10-9 eV/Å. Once the output file is obtained after the vc relax calculation which uses pwscf code for its computation, it is displayed in VESTA and lattice constants are determined. Atomic angles as well as bond lengths are obtained after visualizing in VESTA.

3.2 Energetic Properties

Total energy and binding energies of the monolayers were out obtained from SCF calculations. The binding energies specifically were obtained by subtracting total energies of various atoms from the total energy of the material. To be able to determine whether the novel materials can form spontaneously or not, binding energies we plotted against the varied interlayer separation.

Chapter 4

Results and Discussion

In this Chapter, results of the computational work is analyzed and discussed. Section 4.1 deals with the structural properties of the materials where the materials are visualized in xcrysden and materials identified to be 1T- polymorphs of transition metal disulphides. Also, lattice parameters are calculated and compared with results from other computational and experimental works. Section 4.2 focuses on the electronic properties of the metals. Here, band structure plots are analyzed as well as projected density of states to confirm the 1T-polymorph of transition metal disulphides observed during the structural analysis. Also, the contributions of orbitals in the bonding is analyzed using the projected density of states. Through to section 4.3, the energetic properties of the materials are also analyzed from the calculations. Binding energies of the materials are plotted as a function of the inter-layer distance and the minimum binding energy is used to determine whether the materials can be formed spontaneously or not. Also, total energy of the materials are analyzed. Finally in section 4.4, hydrogen evolution reaction is performed on the most stable material and the properties are analyzed after the evolution reaction.

4.1 Structural Properties of Transition Metal Disulphides

Quantum espresso implementation of Density functional theory (DFT) was used for the computation of structural and electronic properties of monolayer and hetero-structures of 1T prototypes of transition metal disulphides namely PdS2, WS2, ReS2, ReS2-WS2, MoS2-WS2, PdS2-WS2, ReS2-PdS2. The Generalized Gradient Approximation (GGA) of the exchange correlation energy and pseudopotentials

were applied to these calculations. Brillouin zone sampling was also done using the Monkhorst-Pack approach where 14x14x2 and 16x16x2 was used for the monolayer and hetero-structures respectively. We first performed variable-cell relaxation computation for all the materials to obtain the optimized lattice parameters of these materials where the results are discussed in section 4.1 below.

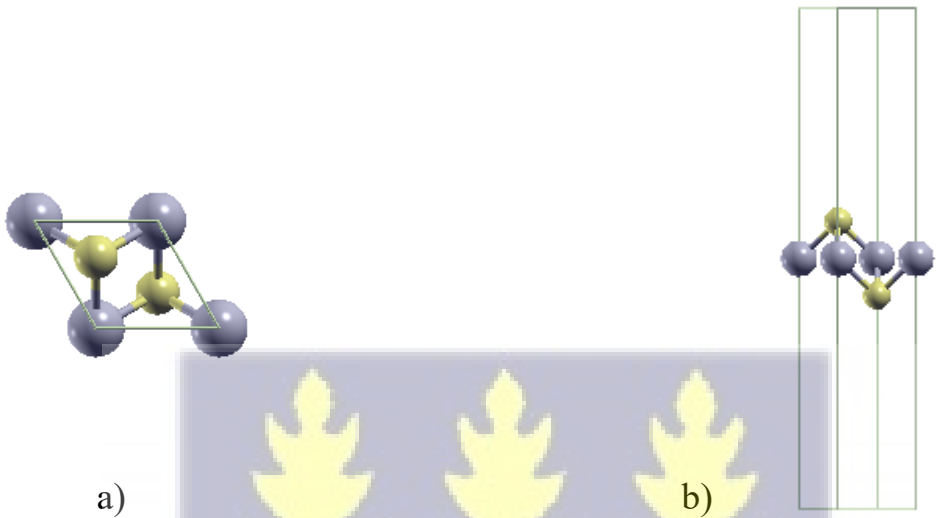

Figure 4.1 a) top view and b) side view of monolayer transition metal disulphides (Sulphur (pale yellow) transition metal(dark-grey)

Self-consistency filed(SCF) calculations were performed for all the materials to obtain their total energies. Bulk transition metal disulphides are stacked by monolayers of transition metal disulphides through Van-der-Waal forces. Therefore, to understand the structure of transition metal disulphides we need to carefully study their monolayers first. The monolayers of transition metal disulphides as shown in Figure 4.1 reveals that in the structure, one transition metal is sandwiched between the two layers of the Sulphur in a V-shape. The bonds between the transition metal and the Sulphur atoms is covalent bonds and therefore makes it stable. The 1T prototypes of monolayers including MoS_2, PdS_2, ReS_2 and WS_2 were considered in this project. The monolayers were created with a vertical gap of roughly 25Å between the

unit cells so as to separate each layer from interacting with its periodic image. Optimization calculations have been performed on the materials using Quantum Espresso. For the calculations, a k-point mesh of 14x14x1 was used for the Ultra Soft Pseudo-potential, cut off of 50 Rydberg was used and relax calculation to obtain optimized lattice parameters by visualizing materials in VESTA.

Starting off with PdS_2, the monolayer structure of PdS_2 used in this work exhibits the 1T-phase with a lattice constant a=3.55165 Å b= 3.55165 Å which agrees with experimental data. The structure of PdS_2 used in this work exhibits an octahedral coordination and a tetragonal symmetry with only one S-Pd-S as a repeat cell. The S-Pd-S bonding angles are all 65 degrees with average Pd-S bond length of 3.28629 Å. Atomic structure of ReS_2 monolayer is also in the 1T phase. The magnetic structure is triclinic with a P1 space group symmetry. The calculated optimized lattice constants are a=3.01211 Å b=3.01211Å which agrees with referenced works. The Re-S bond length is 2.40228 Å with bond angle 38.6875 degrees. Calculated optimized lattice parameter for WS_2 is a=3.24320Å b= 3.24320Å with W-S bond length of 2.42218Å and bind angle 38.6875 degrees. The structure of WS2 also exhibits 1T phase. ReS2 monolayer can exist in 1H or 1T structures. For this work, 1T structure is used as it is preferred over the 1H prototypes per previous studies. The calculated lattice constants are a=6.31211Å and b= 6.31211Å which agrees with values in previous work (Mahler et al., 2014)

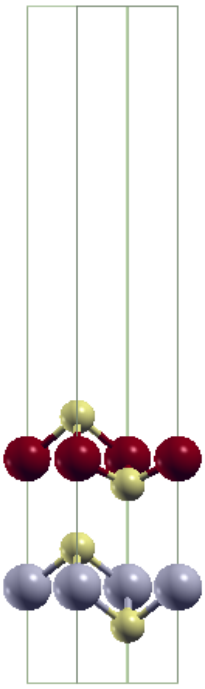

a)

b)

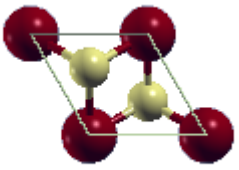

c)

Figure 4.2 a) x-z plane b) y-z plane c)x-y place orientation of the hetero-structures. Sulphur (Pale- yellow) transition metals represented in (wine and dark-grey colors).

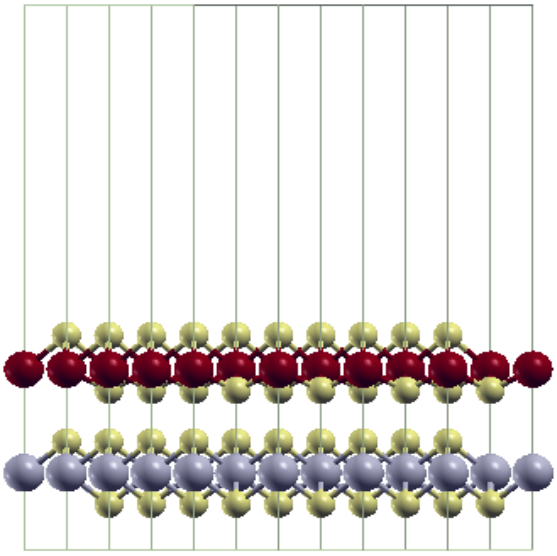

4.3a

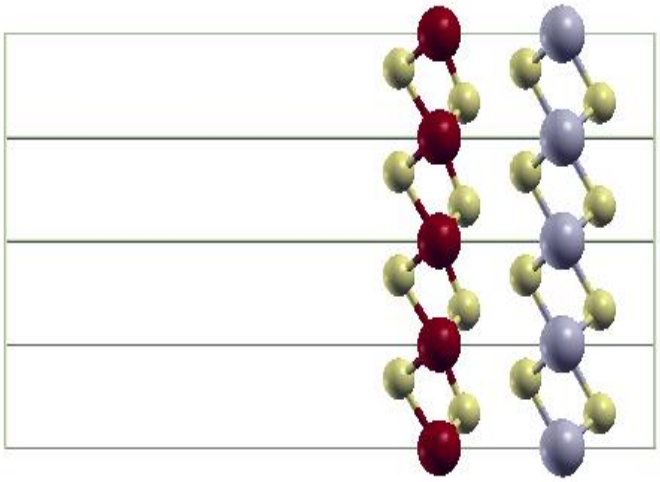

4.3b

Figure 4.3 a) x-z plane b) y-z plane of optimized 4x4x1 hetero-structure of transition metal disulphides. Sulphur (Pale-yellow) transition metals represented in (wine and dark-grey colors).

The hetero-structures of these transition metal disulphides are formed by placing one layer of material on top of another material in the AA stacking mode. New hetero-structures from the 1T- monolayers of MoS_2, PdS_2, ReS_2 and WS_2. These hetero structures namely MoS_2-PdS_2, WS_2-PdS_2, ReS_2-PdS_2, ReS_2-WS_2, MoS_2-WS_2 were created by AA stacking modes as shown in Figure 4.3a above. The visualized image in Figure 4.3a and b shows that the hetero structures are formed by placing a layer of one transition metal disulphides of another. For example, in the case of MoS_2-PdS_2, PdS_2 monolayer is placed on MoS2 monolayer and the inter layer spacing distance between them corresponds to the minimum energy. In the creation of the hetero-structures, we have tested PBE-Sol/GGA functional. Self-consistency field calculations have been performed on the materials created in Quantum Espresso whiles the inter layer spacing is varied to achieve the minimum Binding Energy. This is the energy at which the materials will

be formed spontaneously (i.e., in the case of negative minimum binding energy) or formed by adding energy (positive binding energy).

Table 4.1 Theoretically calculated optimized lattice parameters, bond lengths, and the S-TM-S bond angles of monolayer transition metal disulphides and their hetero-structures.

Transition metal disulphides	**2D-crystal system**	**a(Å)**	**b (Å)**	**Interlayer Separation (Å)**	**Bond length**
PdS_2	1T- Trigonal	3.55165	3.55165	Not applicable for monolayer	Not applicable for monolayer
Reference (PdS_2) (Terrones & Terrones,2014)	2H- polytype	3.45671	3.45671	Not applicable for monolayer	Not applicable for monolayer
WS2	1T- polytype	3.24320	3.24320	Not applicable for monolayer	Not applicable for monolayer
Reference (WS_2) (Mahler et al., 2014)	1T, 2H	3.2502	3.2502	Not applicable for monolayer	Not applicable for monolayer
ReS_2	1T-polytype	6.31211	6.31211	Not applicable for monolayer	Not applicable for monolayer
Reference (ReS_2) (Obodo et al., 2019)	1T-polytype	6.40200	6.50700	Not applicable for monolayer	Not applicable for monolayer
ReS_2-WS_2	1T-polytype	3.09925	3.09925	3.10090	2.2087
MoS2-WS2	1T-polytype	3.08925	3.08925	3.09070	2.4657
WS2-PdS2	IT-polytype	3.45450	3.45450	3.10540	2.8802

ReS2-PdS2	1T-polytype	3.21133	3.21133	2.91710	2.3802
MoS2-PdS2	IT-polytype	3.20643	3.230643	2.92530	2.3702

4.2 Energetic Properties of the Transition Metal Disulphides

To confirm the thermodynamic stability of the most stable heterobilayer among all the materials formed recommend the fabrication of the heterostructures based on whether they are energetically feasible or not, we computed the binding energy as a function of the interlayer distance between the two monolayers forming the hetero bilayer.

The binding energy is defined as the total energy per unit hetero structure minus the total energy of the free-standing transition metal disulphides as a function of the distance between the top and bottom layer transition metal sulphides. Considering MoS_2-PdS_2, the binding energy is defined below

$$\text{B.E (Mo}S_2\text{-Pd}S_2\text{)} = E_{total}\ (\text{Mo}S_2\text{-Pd}S_2) - E_{total}\ (\text{Mo}S_2) - E_{total}\ (\text{Pd}S_2).$$

Binding energies alongside the interlayer distance are illustrated in Table 4.2

The resulting MoS_2-PdS_2 double layer gives an equilibrium distance of 2. 2.93Å and an equilibrium binding energy of -0.26eV as shown in Figure 4.1. WS_2 -PdS_2 and ReS_2 -PdS_2 have higher binding energies compared to MoS_2-PdS_2 as seen in Figures 4.2 and 4.3. The negative binding energy for all MoS_2-PdS_2, WS_2-PdS_2 and ReS_2-PdS_2 also recommends the fabrication of the heterostructures as they can be formed spontaneously. The equilibrium interlayer distance at approximately 2.9 Å verifies Van der Waal's interactions between these layers.

MoS_2-WS_2 and WS_2-ReS_2 cannot be formed spontaneously due to their positive equilibrium binding energy as shown in Figures 4.4 and 4.5.

Table 4.2 Binding Energy (E_b/ eV) and interlayer distance (d/ Å) for different bilayer heterostructures.

1T-bilayer heterostructures	MoS_2-PdS_2	PdS_2-WS_2	ReS_2-PdS_2	ReS_2-WS_2	MoS_2-WS_2
Binding Energy (E_b/eV)	-0.26	-0.49	-0.35	0.41	0.25
Interlayer distance (d/Å)	2.93	3.10	3.11	3.09	3.13

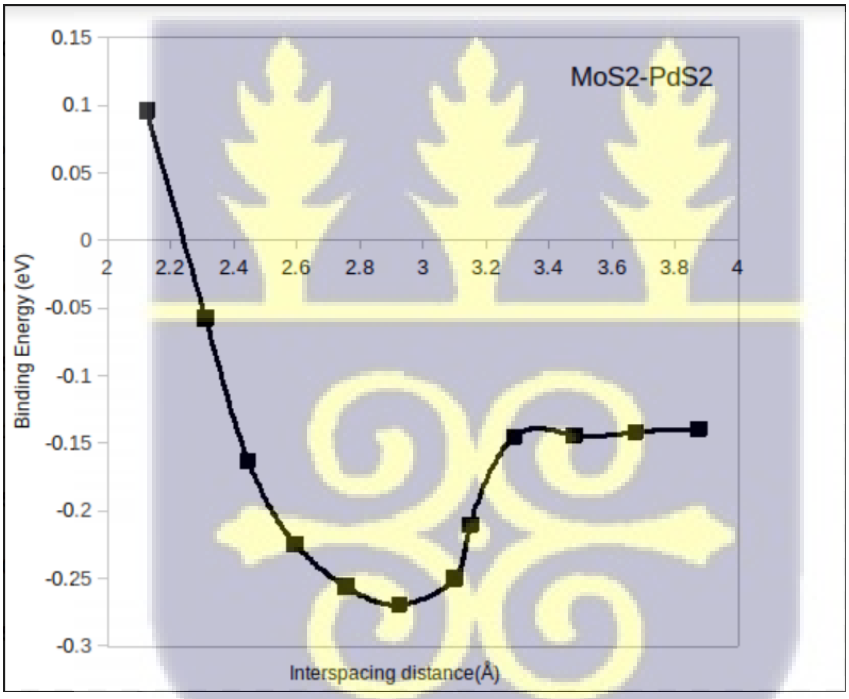

Figure 4.1 Binding Energy curve of MoS_2-PdS_2 versus the inter-spacing distance between MoS_2 and PdS_2 layers.

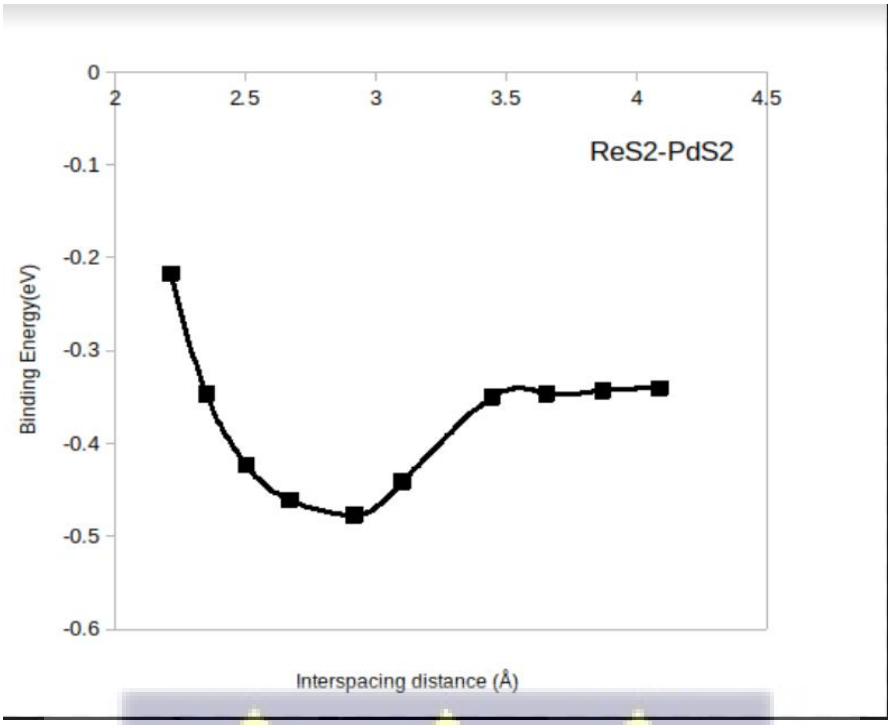

Figure 4.2 Binding Energy curve of ReS_2-PdS_2 versus the inter-spacing distance between ReS_2 and PdS_2 layers.

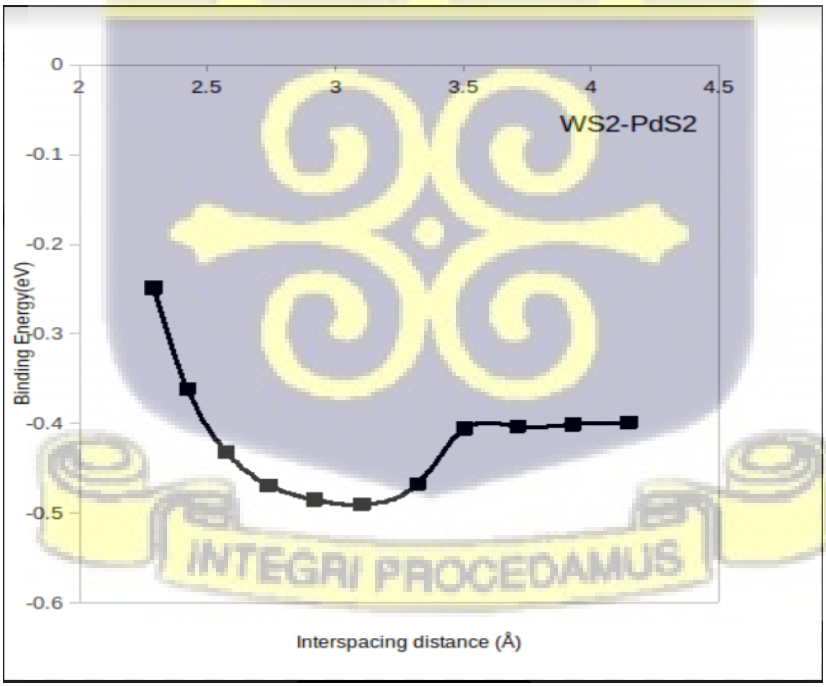

Figure 4.3 Binding Energy curve of WS_2-PdS_2 versus the inter-spacing distance between WS_2 and PdS_2 layers.

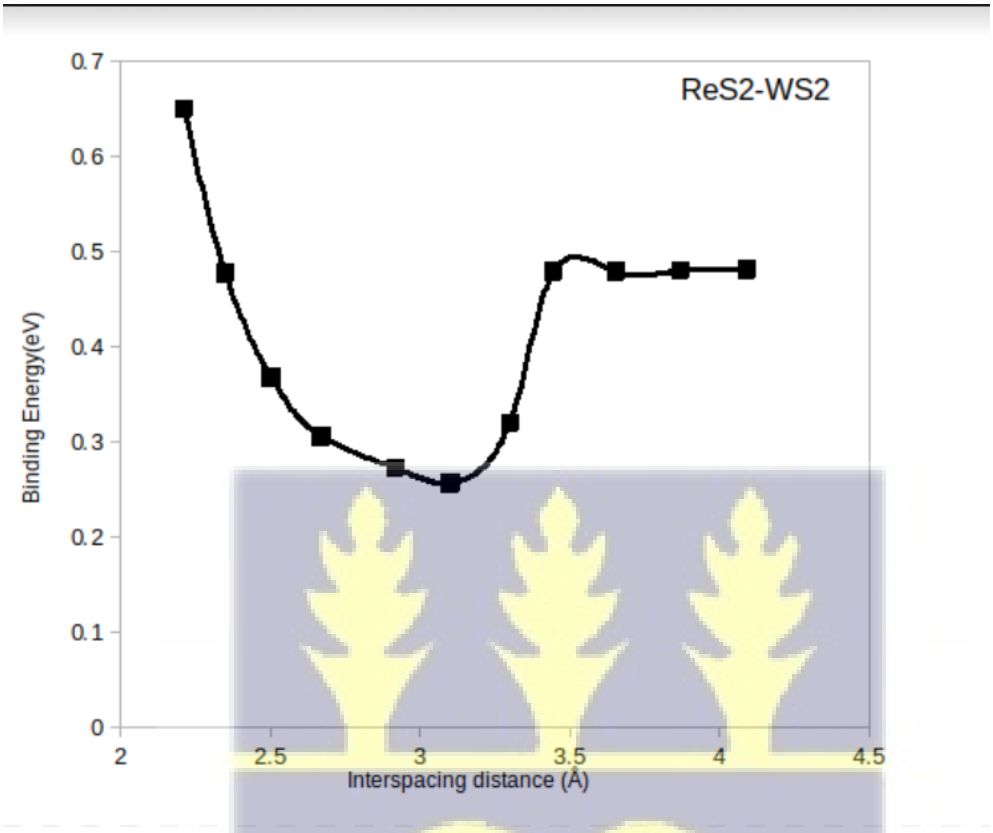

Figure 4.4 Binding Energy curve of WS_2-ReS_2 versus the inter-spacing distance between WS_2 and ReS_2

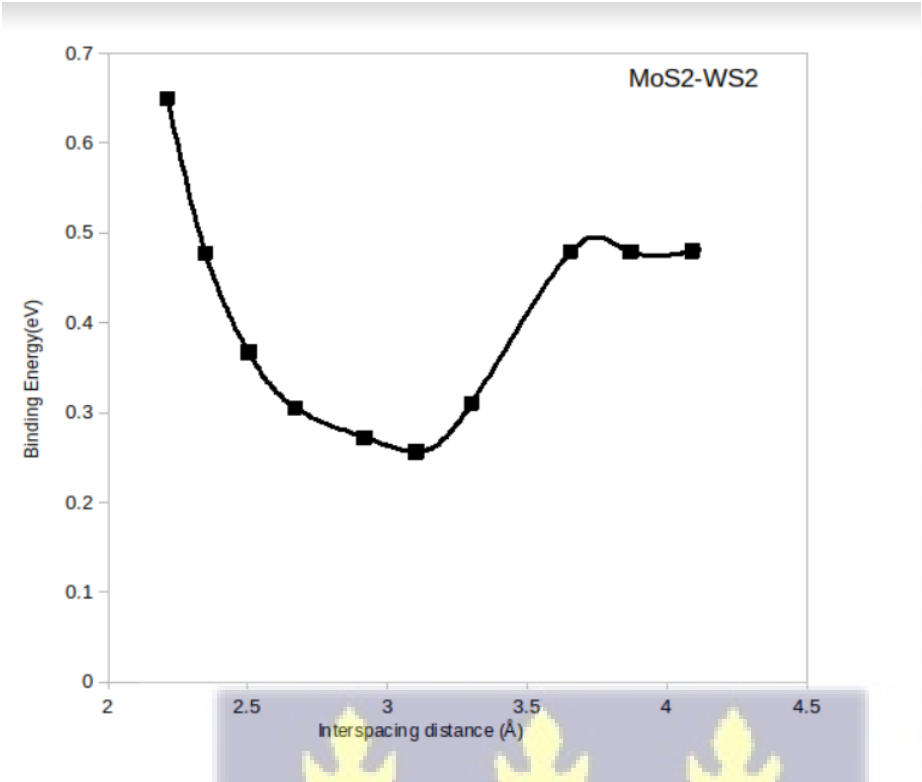

Figure 4.5 Binding Energy curve of MoS_2-WS_2 versus the inter-spacing distance between WS_2 and MoS_2

4.2 Electronic Properties of Transition Metal Disulphides

The electronic properties including band structure and partial density of states have been analyzed in below discussions. The band.x and projwfc.x in Quantum Espresso has been applied to calculate the band structure and partial density of states respectively (Giannozzi et al., 2009)

4.3 Monolayer Transition Metal Disulphides

For 1T-WS_2, it can be observed that the valence and conduction band contributions to the 1T-WS_2 monolayer consist of W-d states and S-p states consistent with previous work by (…..).

A careful study of the orbitals also reveals that, there is a large overlap between the Sulphur -p states and the W-d states which suggests a strong covalent bond between the W and S atoms. Also, strong peaks are observed at the fermi-energy level with a range between 0.6 eV in Figure 4.7. There is a very small (almost negligible) contribution of W-s states and no contribution from S-states and there it can be concluded the S-s and W-s do not contribute to the bonding and anti-bonding.

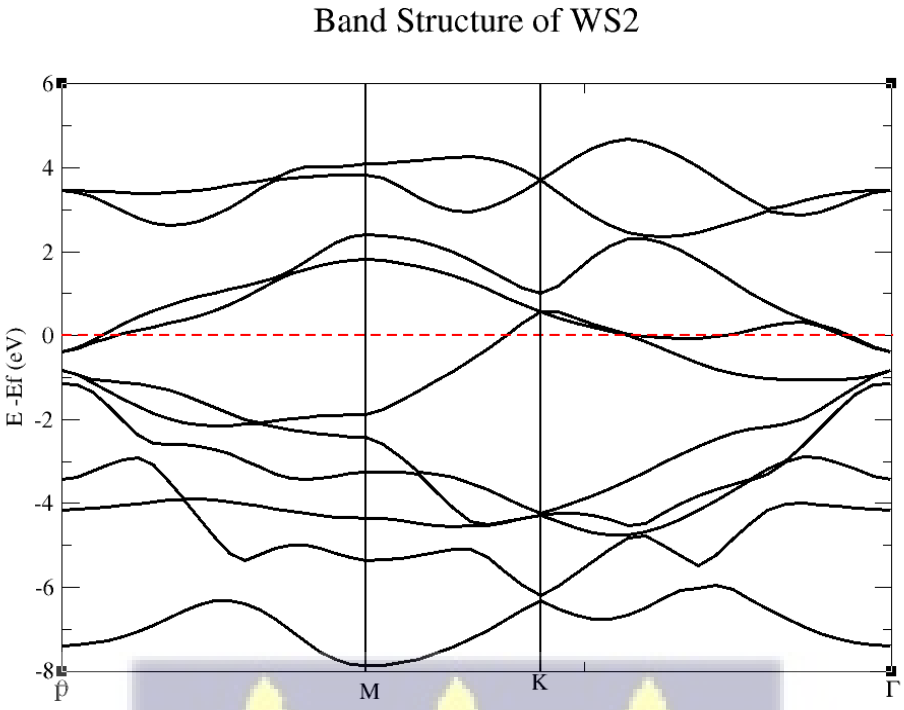

Fig 4.6 Electronic band structure of 1T-WS_2

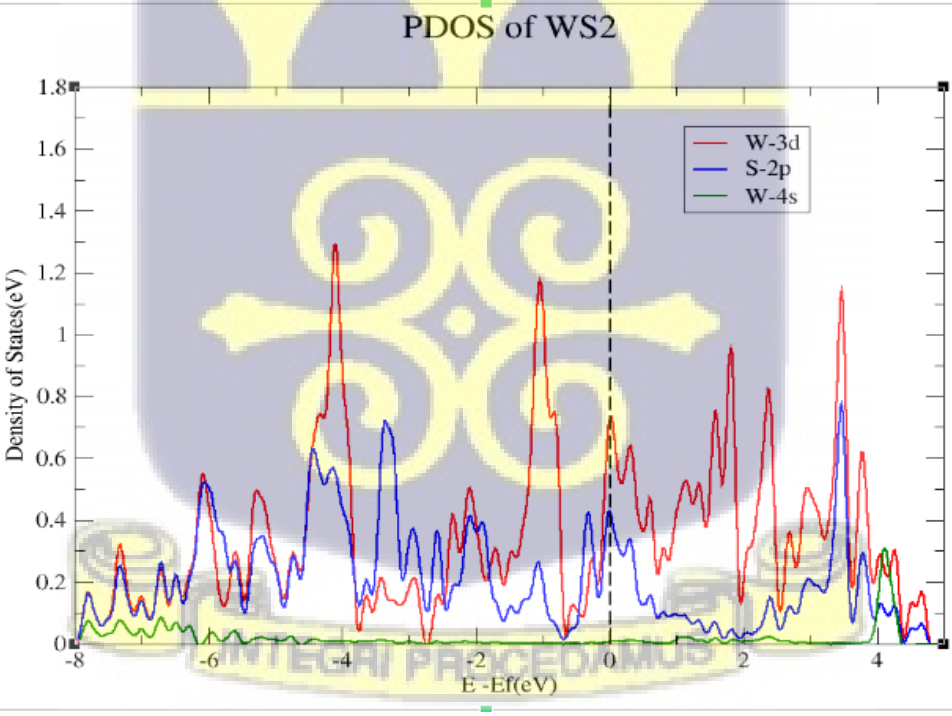

Fig 4.7 Partial Density of states of 1T-WS_2 (Fermi level is at 0)

Unlike 1T-WS_2, ReS_2 displays double crossing above the fermi level with a direct band gap of 0.5eV above the Fermi level between K and Gamma high symmetry points. A study of the partial density of states calculations shows that both transition metal and Sulphides contribute to the electronic states in the valence and conduction band just as it was found in the case of 1T-WS_2. Similarly, a case of strong overlap between the Re-3d states and S-2p states suggests a strong covalent bond between the atoms. The majority contributions of electronic states are the Re-3d states.

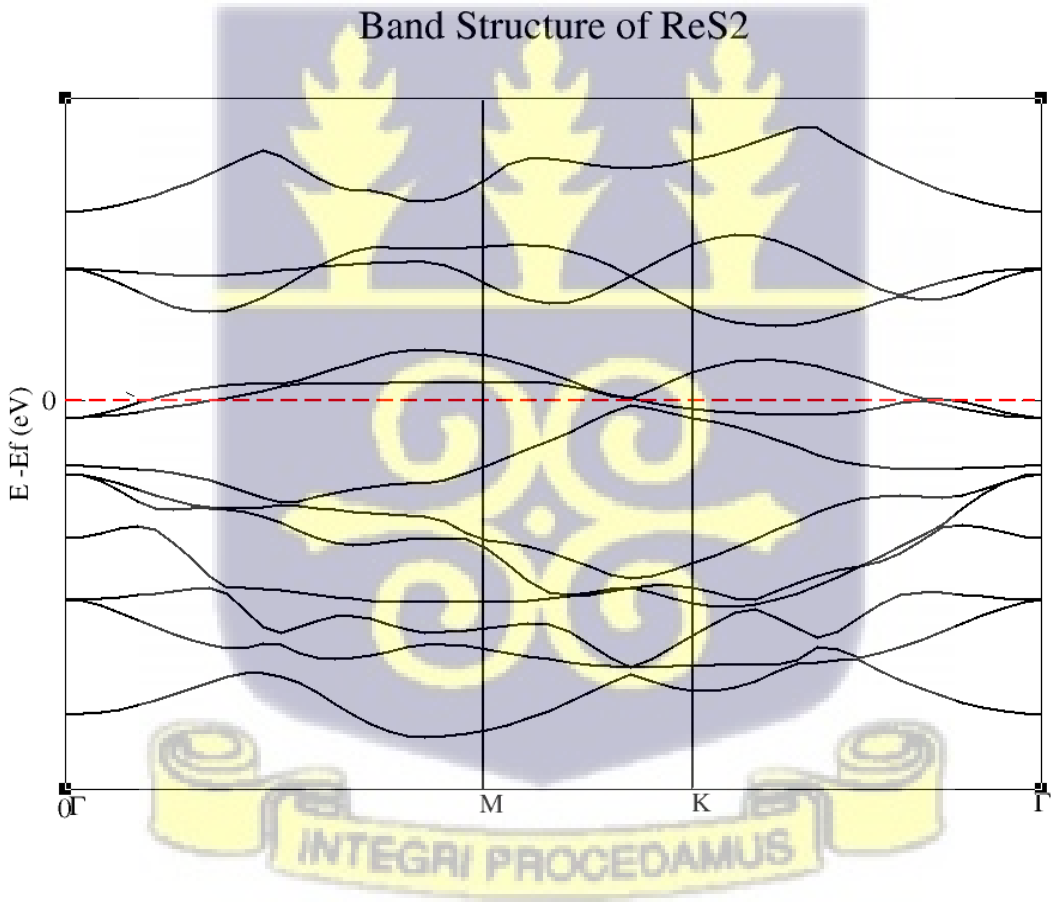

Figure 4.8 Electronic band structure of 1T-ReS_2

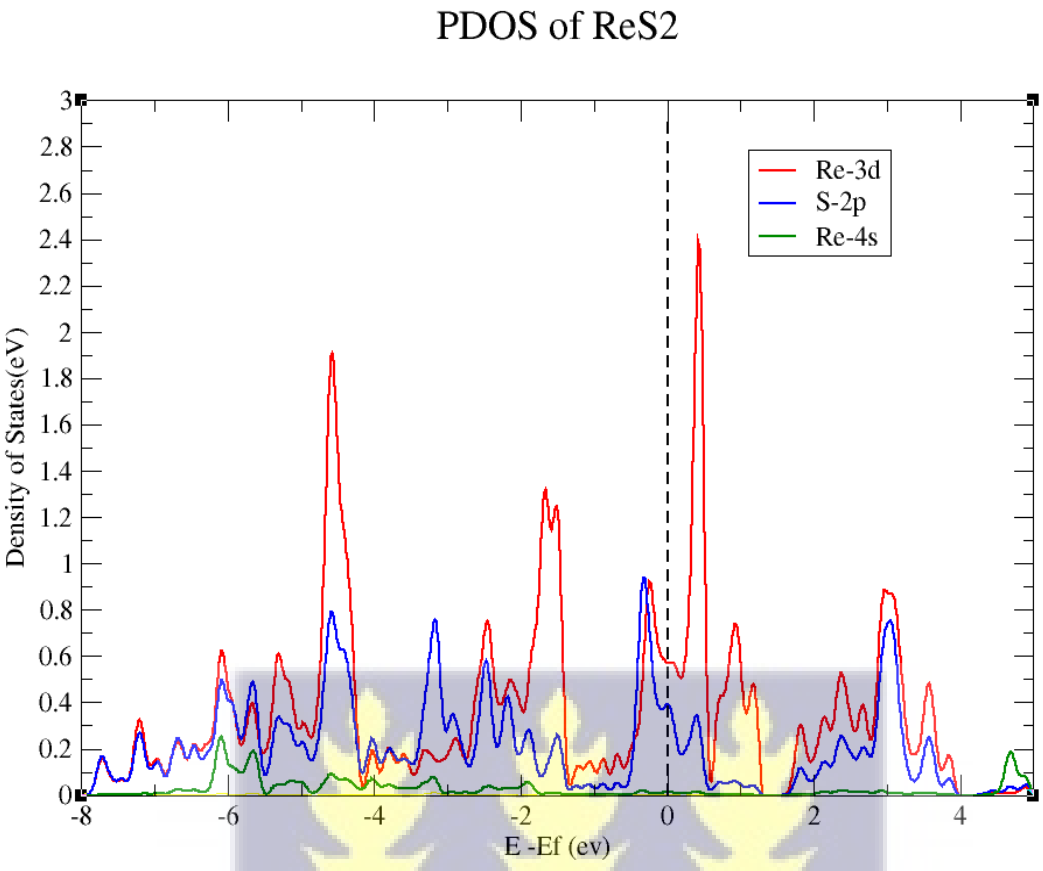

Figure 4.9 Partial Density of states of 1T-ReS_2 (Fermi level at 0)

MoS_2 has been widely studied in its 1T and 2H forms. The band structure obtained from 1T-polytype of the MoS_2 agrees with previous work. (Hai He et., al) A study of the band structure reveals the material is metallic as there is a double band crossing above the Fermi level.

4.4 Hetero bilayers of transition metal disulphides

The hetero-bilayers of 1T-polymorphs of the transition metal disulphides all used in this was found to exhibit metallic properties. It is, therefore, more important to study their electronic properties by analyzing the band structure and density of states.

The bands of 1T-MoS_2-PdS_2 presented in Figure 4.10 are highly two-dimensional. Only one band crosses the Fermi level, and that band is derived from the MoS_2 planes. The hetero bilayer also exhibits an interpenetration of band structure above the Fermi level. The total and partial density of states for 1T-MoS_2-PdS_2 are plotted in Figure 4.11 A sharp peak of about 2.5 electrons/eV is observed at the fermi level with the partial contribution of electrons originating from largely Mo-4d states and hybridization of the S -2p states. Here the contribution of Pd states at the fermi level is insignificant.

Also, there is an overlap of d-states of the transition metals (Mo and Pd) below and farther away from the fermi level between -6eV and -3.5eV. This overlap explains the evidence of Van der Waal interaction between the hetero- bilayers as already discussed in theory.

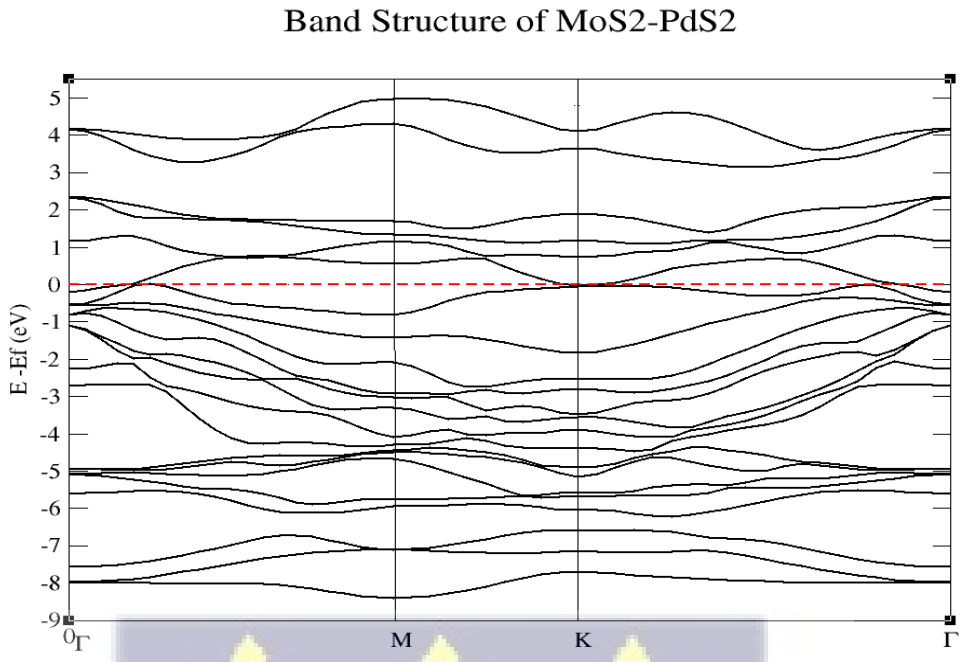

Figure 4.10 Electronic Band Structure of heterostructure of 1T-MoS_2-PdS_2

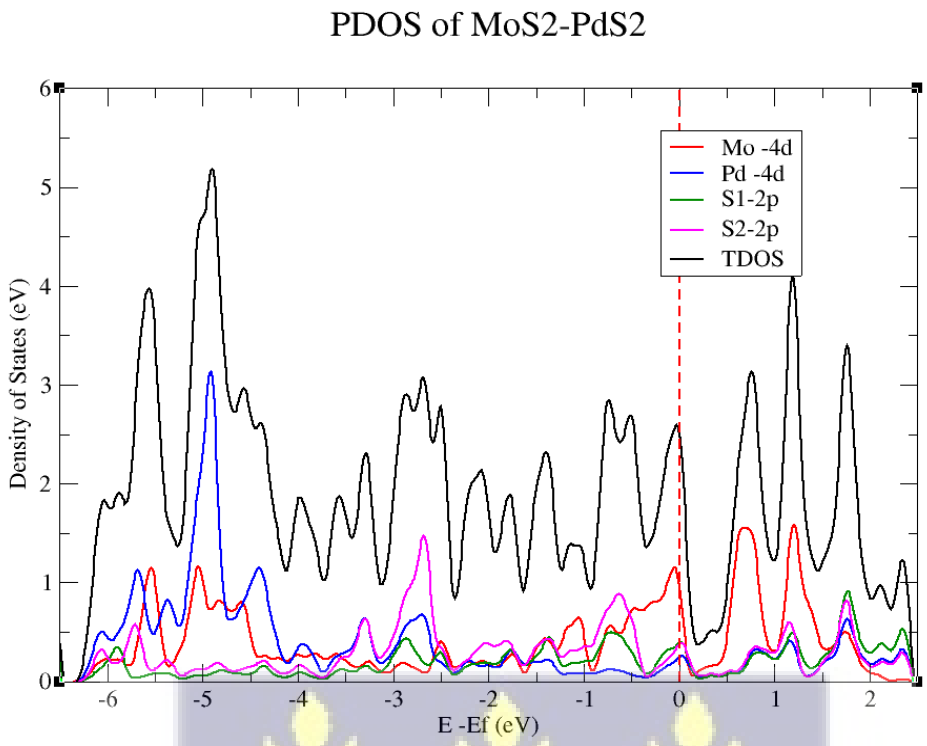

Figure 4.11 Partial density of states of 1T hetero bilayer of MoS2-PdS2

The band structure of WS_2-PdS_2 also shows only one band that crosses the fermi level. Unlike the the MoS_2-PdS_2, no interpenetration of bands is observed above the Fermi level, rather, two very small direct band gaps with energies 0.15eV and 0.20 eV are observed between Gamma, M high symmetry points and K, Gamma high symmetry points respectively. The total and partial density of states have also been computed to show that, the electronic states at the Fermi level for WS_2 -PdS_2 are slightly due to the W-3d states. This scenario where there is a crossing of a band above the Fermi level and almost touching of bands occurs may give rise to a new type of unique material called "Semimetal" in transition metal disulphides when doping or defects cause a shift to the bands to the touching or overlap area. Unlike the MoS_2-PdS_2 where an overlap is observed between the transition metals, there is almost no overlap between the W and Pd -d states.

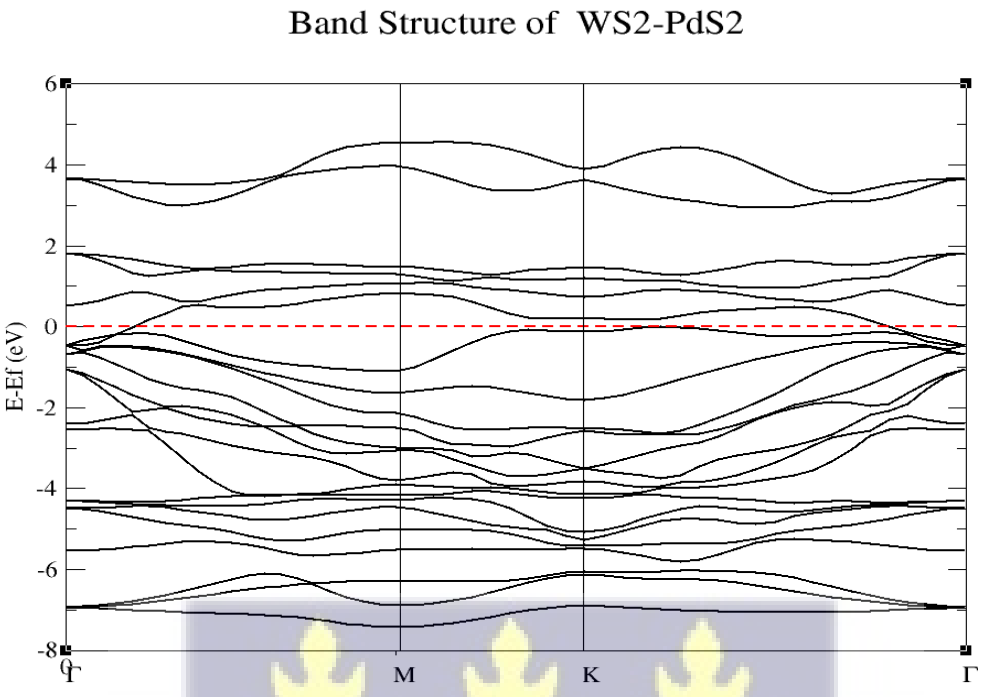

Figure 4.12 Electronic Band Structure of WS2-PdS2

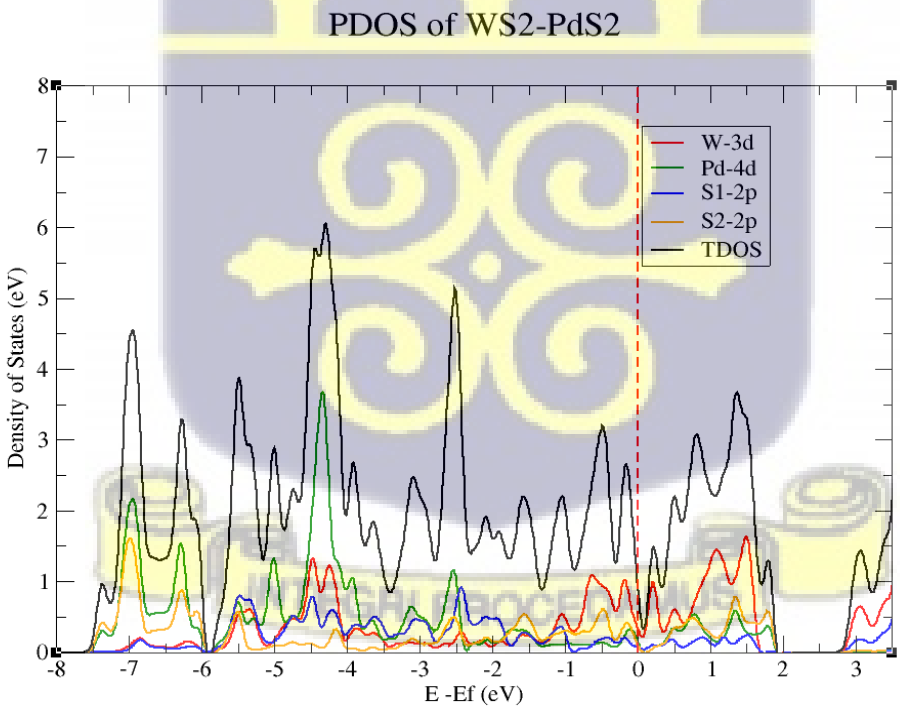

Figure 4.13 Partial Density of States of 1T-hetero bilayer WS2-PdS2

Band structure analysis of PdS_2-ReS2 also shows a single band crossing above the fermi level and interpenetrating the band closer to the fermi level in the conduction band. For the partial density of states of PdS_2 -ReS_2, Pd -4d and Re-3d states mainly contribute to the lower part of the valence band. The upper part of the valence band has mainly the contributions of Re-3d states and slightly that of S-2p states very close to the fermi level. Most electronic states in the conduction band close to the fermi level is mainly Re-3d states. Compared to MoS_2 -PdS_2, PdS_2 -WS_2, there is a similarity in the band structure as in all cases, there is a single band crossing above the fermi level. Also, in all case the transition metals have the highest electronic contribution near the Fermi level.

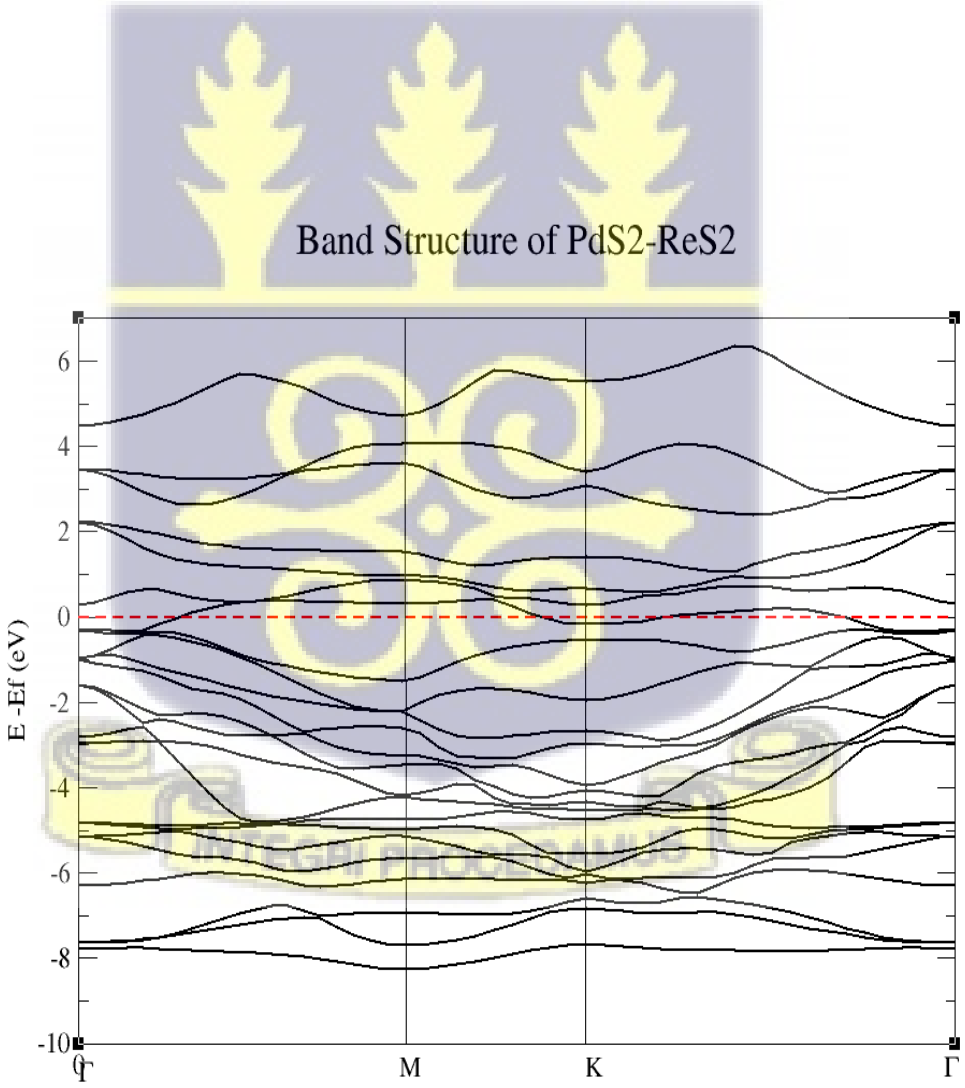

Figure 4.14 Electronic Band Structure of 1T-hetero bilayer WS_2 -PdS_2

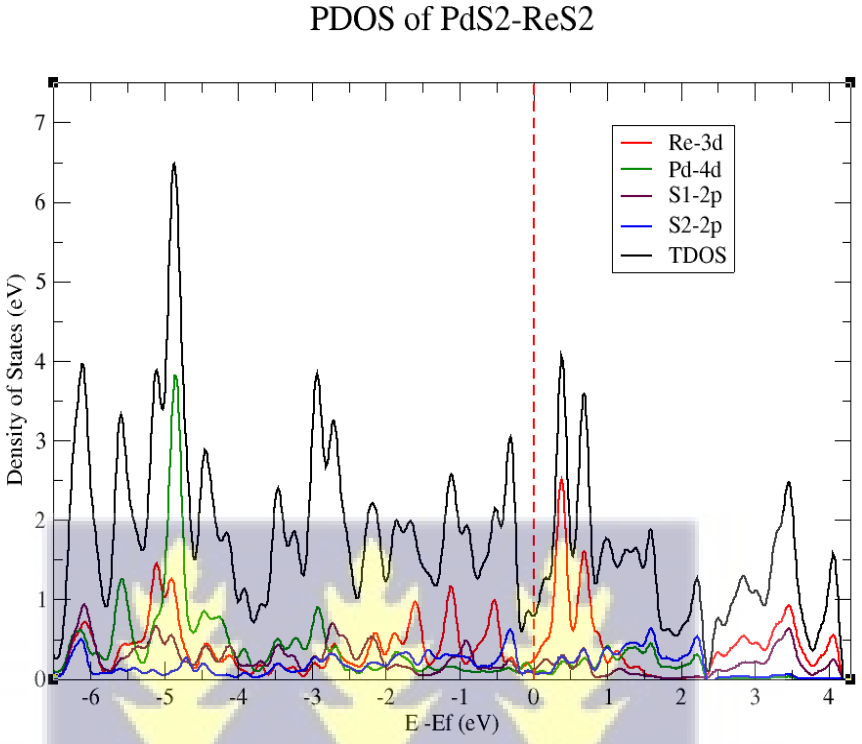

Figure 4.15 Partial Density of States of 1T-hetero bilayer PdS_2 -ReS_2

MoS_2 -WS_2 has a band structure where the is a crossing of three bands above the fermi level unlike the other materials which has one band crossing. There is a small indirect band gap of 0.05ev around 0.5eV between K and Gamma high symmetry points. The total density of states has been computed to show 1.35 electronic states/eV with the highest partial contribution of Mo-4d states and an a hybrid states of W-3d, S-2p states at the fermi level. Below and above the fermi level shows a complete hybridization of Mo-4d, W-3d and S-2p states simultaneously with peaks of the transition metals Mo-4d states and W-3d states very near to the Fermi level. The strong overlap of Mo-d, W-3d and S-2p states suggests there may be the presence of strong covalent bonds between the atoms. Also, the almost touching of bands above the fermi level suggests doping or defects may shift the fermi level to the band touching area leading to a new "semi-metal" feature in this hetero-bilayer of 1T- transition metal disulphides.

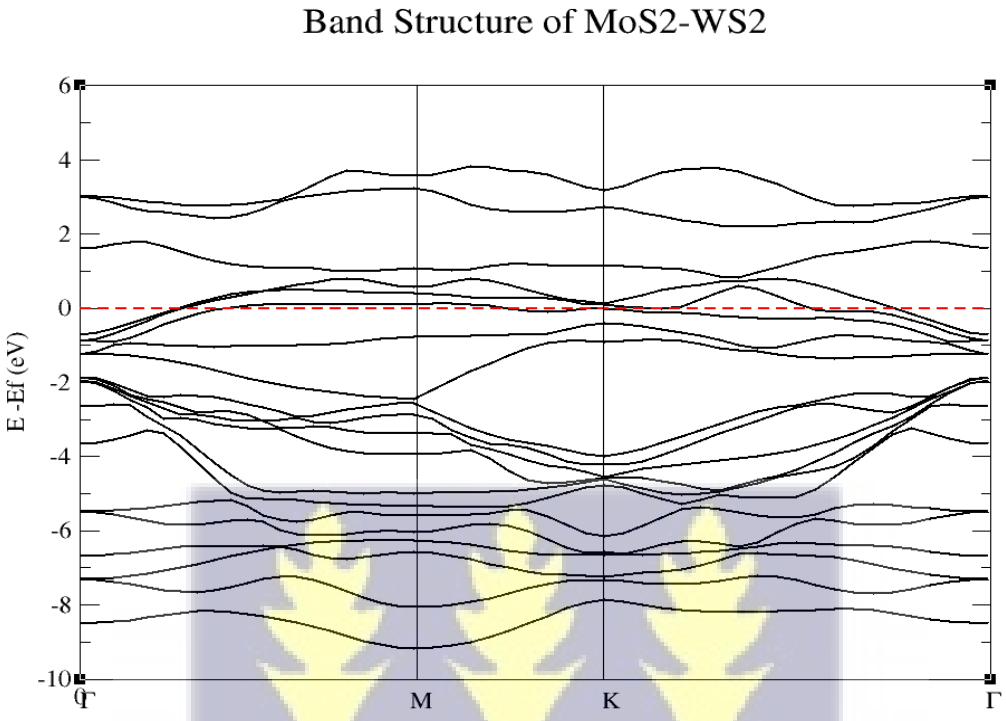

Figure 4.16 Electronic Band Structure of 1T-hetero bilayer MoS_2 -WS_2

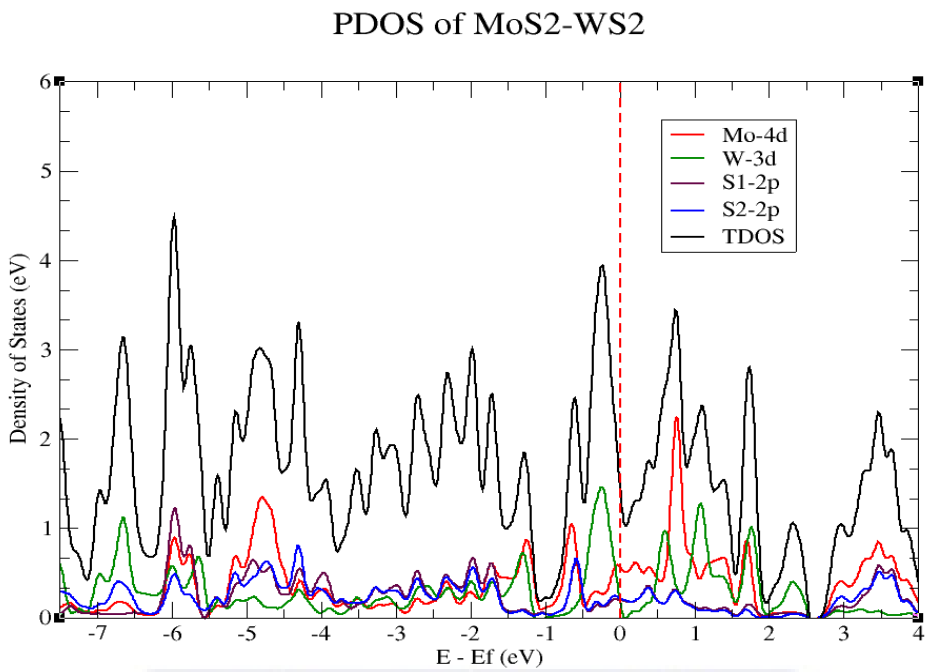

Figure 4.17 Partial Density of States of 1T-hetero bilayer MoS_2 -WS_2

4.5 Hydrogen Adsorption on Selected hetero bilayer (WS_2 - PdS_2)

As previously mentioned, the hydrogen evolution reaction (HER) can proceed through either the Volmer-Tafel or the Volmer-Heyrovsky mechanisms. HER may encounter restrictions from either the Volmer or Tafel/Heyrovsky responses along these two pathways. The primary factor influencing this is the adsorption of hydrogen on the catalyst's surface. The energy associated with hydrogen adsorption (ΔE_{ads}) is calculated using the formula:

$$\Delta E_{ads} = \Delta E_{s+nH} - E_s - \frac{n}{2} E_{H_2} \quad (43)$$

Where ΔE_{ads} is the calculated total energy , E_s is the total energy of the system without the adsorbed hydrogen n is the number of hydrogen (in this case $n = 1$)

Inserting ΔE_{ads} into the equation and using $\Delta E_{ZPE} = 0.04\ eV$ (as calculated by Norskov et al., 2005, representing all transition metals) along with $\Delta S_H^0 \approx \frac{1}{2}\Delta S_{H_2}^0 = 0.2eV$ (where $\Delta S_{H_2}^0$ is the entropy of H_2 in the gas phase at standard conditions), simplifies the equation

$$\Delta G_H = \Delta E_{ads} + 0.24eV \quad (44)$$

Given that hydrogen may be adsorbed at various sites, the hydrogen atom (H) was initially positioned on top of the heterostructure, and its atomic position was allowed to relax without constraints along the x,y, or z axes. The atomic positions of the atoms were similarly allowed to relax while maintaining a constant interlayer distance of 25 Å.

The calculated Gibbs free energy is 0.13 eV, while the energy of formation is -0.11 eV.

Table 3 Energy of Formation and Adsorption Free Energy of Hydrogen for 1T WS_2 -PdS_2

Material	Energy of Formation (eV)	Adsorption Free Energy ΔG_H/eV
1T WS_2 -PdS_2	-0.11	0.13

The above result with adsorption free energy 0.13eV and energy of formation -0.11eV for surface adsorbed hydrogen on 1T- WS_2 -PdS_2 shows the configuration of the material is good for hydrogen evolution reaction.

Chapter 5

Conclusion and Future Perspective

Several novel bilayers of heterostructures of monolayer 1T–polytypes of MoS_2, ReS_2, PdS_2 and WS_2 using first principle calculations have been investigated. Remarkably, a review of the structural properties reveals an octahedral coordination which suggests that the materials are 1T-polytypes of transition metal disulphides. Relax calculations implemented in Quantum Espresso were performed on the monolayers to calculate their optimized lattice parameters. It was found that the calculated lattice parameters agreed with theoretical and experimental results in previous studies. Bilayer heterostructures of the monolayers including MoS_2 -PdS_2, WS_2 -PdS_2, ReS_2 -PdS_2, MoS_2 -WS_2, ReS_2 -WS_2 were formed placing one monolayer on top of the other in AA stacking mode. The interlayer distance between the two monolayers was varied against the binding energy to obtain the minimum binding energy at which the material may be formed either spontaneously or by adding sufficient energy to create the material. Further analysis of the minimum binding energies of these bilayer heterostructures shows MoS_2 -PdS_2 can be spontaneously formed easily by releasing energy followed by WS_2 -PdS_2 and PdS_2 -ReS_2. MoS_2 -WS_2 and ReS_2 -WS_2 tend to have negative binding energy which implies they cannot be formed spontaneously. Also, it was found that the average minimum interlayer distance was found to be 3.0 Å which verifies the Van der Waals interaction between the two layers.

The electronic properties of the 1T crystals have also been investigated using first principle calculations. Band structure, total and partial density of states have been calculated, analyzed, and compared for the all the 1T crystals including the monolayers and bilayer heterostructures. The band structure of the1T monolayer crystals of MoS_2, WS_2, ReS_2 and PdS_2 were all metallic due to the crossing on bands above the fermi levels. Also, a strong overlap of the transition metal d-states promises a strong covalent bond

between the atoms. For the bilayer heterostructures, MoS_2 -PdS_2 is identified as most stable and can be easily formed spontaneously. Its band structure reveals band cross from the conduction band above the fermi and interpenetration with the conduction bands suggesting a highly metallic, large surface area and high electrical conductivity making them suitable for an excellent hydrogen evolution reaction catalyst. The partial contribution of electronic states shows an overlap between the 4d and 3d states of Mo and Pd respectively which explains the evidence of Van der Waal's interaction between the bilayer heterojunctions.

MoS_2-WS_2 and WS_2-PdS_2 which is the next material to be easily formed spontaneously due to their negative minimum binding energy have a band structure where there is a crossing of the band above the fermi level with no interpenetration but rather an almost touching of bands in the conduction bands. This is known to give rise to a new type of semimetal unique when the material is doped, or defects cause a shift of the fermi level to the bands touching area.

These novel metallic 1T-bilayer heterostructures promise a future low-cost catalyst or cocatalysts for hydrogen evolution reactions in the future if it is explored. Several exploration methods may include 1T/2H mixed phase of the heterostructures, defects engineering and doping.

References

Blöchl P. E. (1994). Projector augmented-wave method. *Physical Review B*, *50*(24), 17953–17979. https://doi.org/10.1103/PhysRevB.50.17953

Cai, L., Cheng, W., Yao, T., Huang, Y., Tang, F., Liu, Q., Liu, W., Sun, Z., Hu, F., Jiang, Y., Yan, W., & Wei, S. (2017). High-Content Metallic 1T Phase in MoS2-Based Electrocatalyst for Efficient Hydrogen Evolution. *Journal of Physical Chemistry C*, *121*(28), 15071–15077. https://doi.org/10.1021/acs.jpcc.7b03103

Garrity, K. F., Bennett, J. W., Rabe, K. M., & Vanderbilt, D. (2014). Pseudopotentials for high-throughput DFT calculations. *Computational Materials Science*, *81*, 446–452. https://doi.org/10.1016/j.commatsci.2013.08.053

Giannozzi, P., Baroni, S., Bonini, N., Calandra, M., Car, R., Cavazzoni, C., Ceresoli, D., Chiarotti, G. L., Cococcioni, M., Dabo, I., Dal Corso, A., De Gironcoli, S., Fabris, S., Fratesi, G., Gebauer, R., Gerstmann, U., Gougoussis, C., Kokalj, A., Lazzeri, M., … Wentzcovitch, R. M. (2009). QUANTUM ESPRESSO: A modular and open-source software project for quantum simulations of materials. *Journal of Physics Condensed Matter*, *21*(39). https://doi.org/10.1088/0953-8984/21/39/395502

Kohn, W. (1999). Nobel lecture: Electronic structure of matter - Wave functions and density functional. *Reviews of Modern Physics*, *71*(5), 1253–1266. https://doi.org/10.1103/revmodphys.71.1253

Mahler, B., Hoepfner, V., Liao, K., & Ozin, G. A. (2014). Colloidal synthesis of 1T-WS2 and 2H-WS2 nanosheets: Applications for photocatalytic hydrogen evolution. *Journal of the American Chemical Society*, *136*(40), 14121–14127. https://doi.org/10.1021/ja506261t

Marzari, N., Vanderbilt, D., & Payne, M. C. (1997). Ensemble density-functional theory for ab initio molecular dynamics of metals and finite-temperature insulators. *Physical Review Letters*, *79*(7), 1337–1340. https://doi.org/10.1103/PhysRevLett.79.1337

Payne, M. C., Teter, M. P., Allan, D. C., Arias, T. A., & Joannopoulos, J. D. (1992). Iterative minimization techniques for ab initio total-energy calculations: Molecular dynamics and conjugate gradients. *Reviews of Modern Physics*, *64*(4), 1045–1097. https://doi.org/10.1103/RevModPhys.64.1045

Perdew, J. P., Burke, K., & Ernzerhof, M. (1996). Generalized gradient approximation made simple. *Physical Review Letters*, *77*(18), 3865–3868. https://doi.org/10.1103/PhysRevLett.77.3865

Tan, C., Cao, X., Wu, X. J., He, Q., Yang, J., Zhang, X., Chen, J., Zhao, W., Han, S., Nam, G. H., Sindoro, M., & Zhang, H. (2017). Recent Advances in Ultrathin Two-Dimensional Nanomaterials. *Chemical Reviews*, *117*(9), 6225–6331. https://doi.org/10.1021/acs.chemrev.6b00558

Tang, Q., & Jiang, D. E. (2016). Mechanism of hydrogen evolution reaction on 1T-MoS2 from first principles. *ACS Catalysis*, *6*(8), 4953–4961. https://doi.org/10.1021/acscatal.6b01211

Terrones, H., & Terrones, M. (2014). Bilayers of transition metal dichalcogenides: Different stackings and heterostructures. *Journal of Materials Research*, *29*(3), 373–382. https://doi.org/10.1557/jmr.2013.284

US EIA. (2013). International Energy Outlook 2013 - DOE/EIA-0484(2013). *Outlook 2013*, 312.

Westholm, J., Biplab, S., Co-Supervisor, S., & Puyuelo, R. E. (2018). *First principles calculations of 2D materials*.

Xu, W., Yan, S., & Qiao, W. (2018). Magnetism in monolayer 1T-MoS2 and 1T-MoS2H tuned by strain. *RSC Advances*, *8*(15), 8435–8441. https://doi.org/10.1039/c7ra10304b

Z. W. Seh et al., Two-Dimensional Molybdenum Carbide (MXene) as an Efficient Electrocatalyst for Hydrogen Evolution. ACS Energy Lett. 1, 589-594 (2016).

Jaramillo, T. F., Jørgensen, K. P., Bonde, J., Nielsen, J. H., Horch, S., & Chorkendorff, I. (Year).

Identification of Active Edge Sites for Electrochemical H2 Evolution from MoS2 Nanocatalysts.

Kingsley Onyebuchi Obodo *et al* 2019 *Mater. Res. Express* 6 106307

Novoselov K S, Jiang D, Schedin F, Booth T J, Khotkevich V V, Morozov S V and Geim A K 2005

Two-dimensional atomic crystals PNAS 102 10451